***Final accepted version** – published in Science Robotics as:*

S. A. Burden, T. Libby, K. Jayaram, S. Sponberg, and J. M. Donelan. Why animals can outrun robots. *Science Robotics* 9(89):eadi9754, 2024. DOI:10.1126/scirobotics.adi9754

Title: Why animals can outrun robots

Authors: Samuel A. Burden[1]*†, Thomas Libby[2]†, Kaushik Jayaram[3], Simon Sponberg[4], J. Maxwell Donelan[5]

Affiliations:

[1]Department of Electrical & Computer Engineering, University of Washington; Seattle, WA, 98195, USA

[2]Robotics Laboratory, SRI International; Menlo Park, CA, 94025, USA

[3]Paul M Rady Department of Mechanical Engineering, University of Colorado Boulder; Boulder, CO, 80303, USA

[4]School of Physics, School of Biological Sciences, Georgia Institute of Technology; Atlanta, GA, 30317, USA

[5]Department of Biomedical Physiology & Kinesiology, Simon Fraser University; Burnaby, BC, V5A 1S6, Canada

*Corresponding author. Email: sburden@uw.edu

†Co-first authors.

Abstract: Animals are much better at running than robots. The difference in performance arises in the important dimensions of agility, range, and robustness. To understand the underlying causes for this performance gap, we compare natural and artificial technologies in the five subsystems critical for running: power, frame, actuation, sensing, and control. With few exceptions, engineering technologies meet or exceed the performance of their biological counterparts. We conclude that biology's advantage over engineering arises from better integration of subsystems, and identify four fundamental obstacles that roboticists must overcome. Toward this goal, we highlight promising research directions that have outsized potential to help future running robots achieve animal-level performance.

One-Sentence Summary: Animals use superior integration of inferior components – a bioinspiration principle for transformative advances in robotics.

Main Text:
Animals outperform robots at locomotion. The performance gap is evident across scales, and it is particularly galling since animal designs respect constraints that need not limit robots – for instance, animals must grow from a single cell, repair their own bodies, and contain all the machinery needed to reproduce. We seek to understand the underlying causes for this performance gap by systematically comparing animals to robots.

Although the preceding observations apply to multiple locomotion modalities including flight and swimming, for tractability we focus on legged locomotion, where decades of research have produced a rich robot ecosystem with bio-comparable designs. For succinctness, and to emphasize high-performance behavior, we will use the catchall phrase runner to refer to animals and robots that use intermittent contact between limbs and terrain to move, and running to refer to the corresponding behavior, regardless of whether it would be more common or accurate to describe a behavior as walking or jumping. Toward these ends, we seek to answer the question, "why can animals outrun robots*?*".

Our goal is motivated in part by bioinspiration and biomimetic approaches to design (*1*–*3*), that is, the potential to advance robotics by translating natural to artificial technology, as well as robot-inspired approaches to biology (*4*) and physics (*5*), wherein robots are used to advance basic science. Quantifying the performance of "proof-of-concept'' designs embodied by extant animals sets aspirational benchmarks for the robotics community, highlights performance limiters, and potentially reveals design principles. We expect this study will help catalyze advancements in bioinspired and biohybrid robotics and extremes of performance achievable by autonomous robots (*6*).

Engineered and biological runners are built differently. Robots are assembled from discrete components at the macro-scale whereas animals are formed from heterogeneous structures grown at the nano-scale. And the two technologies employ different physical phenomena and materials for power, sensing, actuation, and control. But both animals and robots are built to run (among other tasks). Given that this shared objective is achieved using vastly different design paradigms, it is not obvious how to compare animal and robot runners. Thus we consider multiple levels of analysis (*7*, *8*), first by quantifying the performance gap between the systems as a whole as in Fig. 1, and subsequently by comparing performance across the five subsystems critical for the task of running illustrated in Fig. 2. Finally, we conclude by synthesizing our findings to propose fruitful future directions for running robot research.

In the following subsections, we compare performance measurements from the literature on animal physiology and robot design. The metrics we choose are largely scale invariant, at least above a minimum size where engineered systems struggle, and are measured in diverse taxa, including vertebrates, invertebrates, and robots. We exclude technologies not integrated into existing autonomous runners, for instance: spider silk is very strong, but it is not employed as a structural material in animal locomotion; nuclear reactors can power submarines but have not been integrated into running robots.

A true meta-analysis remains out of reach because we found no principled weighting by which the performance of such diverse organisms and machines could be distilled into an average value. Instead, we selected data from representative systems to informally assess whether and how biological components exceed the performance of their engineered counterparts; these data are

summarized in Fig. 3. Since a comprehensive metric table with citations would consume this manuscript, we present the details in a supplementary document. We encourage the reader not to skip the supplement, but instead read it for a deeper look at any the component metrics, data, and rationale underpinning our assessments.

System performance

Although the claim that animals outperform robots at running may sound uncontroversial in 2024, it is nevertheless worthwhile to consider how to quantify the performance gap. We think that a runner should have range to operate independently over the distances required, agility to reach and traverse surfaces in its environment, and robustness to maintain range and agility despite changes to the runner and its environment. Although running performance could be measured along other axes, these three non-redundant metrics are commonly studied and of paramount importance for animal fitness and robot autonomy (*9*).

Range can be directly quantified as the distance traveled during autonomous running in a specific environment. This distance is determined by the onboard energy supply as well as the efficiency of energy conversion. The latter factor is conventionally measured by the cost of transport, defined as the amount of energy required to move a unit weight of a runner over a unit distance (*10*). The farthest walk by a legged robot on a single battery charge was Ranger*'s* 65 kilometer trek over the course of 31 hours (*11*). Ranger's cost-of-transport is impressively half that of human walking, but there are important caveats. First of all, the robot's batteries have about 50-fold less useful energy per unit mass as animal fat – the average human has energy reserves to continue walking long after the robot's batteries are depleted. When allowed to refuel along the way, humans can exhibit extraordinary endurance: exceptional athletes can run hundreds of kilometers over multiple days in a single outing. And they can do so over rough terrain whereas Ranger exploits the smoothness of the track it was designed to walk on – a small rock could cause it to stumble and fall. Outside controlled environments, robot range is a distant second to that of animals.

Agility of legged robots has been quantified using running speed, jumping height, turning rate, and more. Legged robot development has long been guided by a need for speed, resulting in bipeds, quadrupeds, and hexapods with speeds approaching those of similarly-sized animals on regular terrain (*12–19*). However, animals are still faster at all scales, and the performance gap widens when considering irregular or deformable terrain (*20*, *21*). Some legged robots have leapt at the task of jumping, either specializing entirely (*22*) or by adapting an existing runner (*23*). New heights have been reached by legged robots using bio-inspired elastic energy storage, but even these are still surpassed by animals of similar mass. Rapid robot turning has been occasionally synthesized (*24*, *25*), but animals can redirect momentum 'on a dime' (*26–31*). Finally, although feedback control can enable robots to recover from substantial perturbations (*32*), the ability of animals in this regard is unmatched (*33*). Overall, animals out-run and out-maneuver running robots.

Robustness is deceptively easy to conceptualize yet devilishly difficult to quantify. As a starting point, we consider how agility and range are maintained in the presence of changes to the runner or its environment. Horses can increase body mass 20-fold as they grow from foal to full size and rhinoceros beetles can carry 30 times body weight without fatiguing. Animals can survive bone fracture (*34*) or limb loss, with many lizards and insects voluntarily shedding appendages to distract predators (*35*), and the phenomenon being so common in the latter group as to motivate a "spare leg hypothesis" (*36*). In contrast, robot range and agility decrease precipitously when large

payloads are added or limbs are damaged. Robots designed to walk or run on flat ground can be made to plod over rough terrain under inclement conditions (*37*), but animals are unimpeded by terrain variations upward of their height (*21*, *38–41*) and readily run over, under, and through obstacles like mud, snow, vegetation, rubble, and crevices (*42*, *43*). On granular media, robot running speed can depend sensitively on design, control, and environmental parameters (*44*), with animals handily outpacing robots in their native ecologies (*20*). Overall, animals excel at maintaining performance despite changes that would be catastrophic for existing robots.

We conclude that animals outperform robots at running along the three key axes of range, agility, and robustness, as illustrated in Fig. 1 and corroborated in other recent work (*45*). In what follows, we seek to understand the cause of this performance gap. Given that animals and robots are generally designed and built using different technologies, it is possible that differences in the parts give rise to differences in the whole. To test this hypothesis, we coarsely divide runners into the five subsystems illustrated in Fig. 2: a power system to store and deliver energy; a frame for support and leverage; actuators to modulate mechanical energy; sensors to perceive self and environment; and a control system to transmit and transform sensor and actuator signals. Of course, our "subsystems" are abstractions and runners cannot always be cleanly divided – particularly in the case of animals. We will take care in what follows to note when separating subsystems is messy work.

Power subsystem performance

The ideal power supply for running stores a large amount of useful energy and delivers it efficiently to the other subsystems with minimal added mass. The three main types of power plants used in autonomous runners are gas engines, electric batteries, and metabolism. All three convert stored chemical energy to power running: engines convert gas to movement; batteries convert chemical bonds to electricity; metabolism converts fat to adenosine triphosphate (ATP).

Since a runner's endurance is ultimately limited by its stored energy, we compare mass-specific stored energy, defined as the energy delivered by the power plant normalized by fuel mass. Biology outperforms engineering by this metric, with values more than double those of combustion engines and 50-fold more than batteries. There are two main reasons for biology's edge: oxidative metabolism within mitochondria converts fat to ATP with a remarkable efficiency of about 70% (*46*), compared to 25% in engines (*47*); and whereas adipose tissue is almost 90% fuel (*48*), gas tanks can be 20% of the mass of the fuel they carry (*49*).

Since locomotion is among the most power-intensive behaviors runners perform, we compare mass-specific delivered power, defined as the sustainable power delivered normalized by total power plant mass. Metabolism meets or exceeds engine performance by this metric (*47*, *50*), but batteries outperform both using the natively high power output of lithium-ion cells and relatively light electronics and packaging. Although animals may transiently achieve higher peak power outputs by depleting the supply of ATP in muscles, the energy in stored ATP is quite limited and, if used on its own, could only sustain performance for a few seconds (*51*, *52*).

Since fuel can potentially be harvested from the environment to extend running distances, we compare mass-specific refueling power, defined as the energy rate of refueling divided by the mass of the refueling frame. By this metric, gas tanks can be refueled an order of magnitude faster than a battery can charge or digestion can process biological matter. To put this in perspective, a human would only need to refuel at the gas rate for a fraction of a second to gain the energy it needs for

each day. The actual human refueling rate limits 100-day running to a range of about 40 km per day (*53*).

In summary, the performance of engineered power plants can exceed that of their biological counterparts in the rates at which they refuel and deliver energy, although biology currently has the edge in energy storage. The development of portable power plants capable of delivering both high specific energy and high specific power is considered one of the grand challenges for mobile robots (*6*). Fortunately, there is no known fundamental barrier to creating engineered power plants that have a superior combination of storage and energy delivering capabilities (*54*).

Frame subsystem performance

The ideal frame for running combines material and geometry to support and propel the body overground while being light and failure-resistant. Running robot frames are generally built from rigid connections between steel, aluminum, or carbon fiber struts using linear or rotary joints. Animal frames have two primary forms: vertebrates have an endoskeleton made from bone connected by soft tissue and insects have an exoskeleton made from hard cuticle connected by soft flexures (*55*). A runner's frame is loaded by multi-axial forces that vary over time (*56*), making it susceptible to multiple modes of failure, including buckling and yielding. Failure modes are affected by the frame's geometric and material properties, and bracing against one failure mode may weaken the frame against another (*57*). A simple yet instructive analysis is to consider a macroshape shared between robot and animal frames (*55*) – a cylindrical tube – and evaluate material resistance to failure modes dominated by stiffness and strength.

Since the body's weight must be supported throughout running without buckling, we compare density-specific stiffness, defined as a material's modulus of elasticity normalized by its density. Carbon fiber outperforms the other materials by this metric by a factor of three to five, with cuticle, bone, aluminum, and steel being roughly comparable. Since limbs must generate large forces to propel the body overground without breaking, we compare density-specific strength, defined as a material's stress before fracture normalized by its density. Carbon fiber again outperforms the other materials by this metric by an order of magnitude; the substantial density of steel makes it the lowest performer in the group. In practical terms, this means a carbon fiber limb could support a heavier body and enable more agile maneuvers that would otherwise break a bone, fracture an exoskeleton, or snap a strut made of aluminum or steel with similar mass.

Since frames and joints often store and return energy, we compare mass-specific energy defined as a material's strength squared normalized by its stiffness and density. In this metric, carbon fiber outperforms the other materials above by a factor of three to ten. However, there are other materials, both engineered and biological, that have exceptional specific energy that can be used for the sole purpose of storing and returning energy. For example, resilin is used in insect jumpers (*58*) and tendon in vertebrates (*59*). Both have higher specific energy than carbon fiber, but not higher than what is achievable by engineered rubber and Kevlar (*60*).

In summary, engineered frames built from carbon fiber can be much stiffer and stronger than biological skeletons built from bone, cuticle, aluminum, or steel; metals may outperform biology with respect to stiffness, but underperform in strength. Animal frames currently exhibit a greater diversity of microshapes (for instance, trabecular bones possess remarkable crack propagation resistance) that offer advantages beyond our metrics (*61*). But a growing catalog of materials and fabrication techniques available to robots may provide similar advantages (*6*, *62*).

Actuation subsystem performance

The ideal actuators for running enable rapid changes in runner momentum with minimal added mass. Animal runners exclusively actuate their limbs with muscle, and most autonomous running robots use electromagnetic motors at vertebrate scales or piezoelectrics at insect scales. The physical principles governing motors, piezos, and muscle are different: motors produce force from the flow of current in a magnetic field, piezos use crystal properties to convert electric fields to mechanical pressure, and muscles produce force through chemical reactions that generate length changes in nano-scale proteins. We exclude other actuators that have been deployed in running robots including hydraulics and artificial muscles (*63*) since motors and piezos are sufficient to justify our quantitative conclusions below.

Since running requires high forces to support the body and move the limbs, we compare mass-specific peak torque, defined as the maximum torque normalized by the mass of the actuator and its transmission. Muscles can outperform direct-drive motors and bimorph piezos (*64*) by a factor of two-to-five in this metric. Although transmissions can theoretically multiply torques by arbitrarily-high gear ratios, the mass added and efficiency lost yields diminishing returns in this metric. Nevertheless, the performance gap between motors and muscles can be eliminated at the vertebrate scale by pairing motors with higher-ratio transmissions like harmonic drives (*65*) or ball screws (*66*) and series compliance to provide backdrivability (*67*).

Since running agility is limited by the rate at which actuator output can be converted to a change in momentum of the runner, we compare mass-specific power, defined as the mean mechanical power over a gait cycle normalized by the mass of the actuator and its transmission. By this metric, peak performance of EM motors exceeds that of muscle by one or more orders of magnitude and piezos are comparable to muscle when used for running. Sustained performance in motors, piezos, and muscles alike is constrained by thermal management and energy supply. Although animals use spring-assisted power amplification to overcome actuator limitations (*68*), robots can also use these mechanisms (*22*).

In summary, the performance of motors with high-ratio transmissions and series compliance can meet or exceed that of muscles in torque and power density, whereas piezos only match muscle in the latter and are at a disadvantage in the former. Motors and piezos have an advantage over muscles in their efficiency of energy transduction which can exceed 90% whereas muscle fiber efficiency in most animals is closer to 30% (under 63% in the most extreme case measured (*69*)). Hydraulic actuators may exceed the torque and power density of motors and muscles, but their efficiencies are often much lower than either, and they require a complex and heavy fluid system in parallel with the electrical systems used for sensing and control. Natural muscles' variable shapes and inherent scalability provide packaging advantages not available in motors, easily adding degrees of freedom where needed, distributing actuation mass elegantly across the body, and providing failure tolerance through redundancy. The diverse linear actuator technologies known as "artificial muscles" may offer similar advantages, but currently have an equally diverse set of limitations compared to motors.

Sensing subsystem performance

The ideal sensor suite for running delivers the actionable information (*70*) needed to move quickly overground. There are two fundamental sensing modalities relevant to running: electromagnetic and mechanical. Eyes, cameras, and lidar are examples of the former; vestibular systems, inertial measurement units, and force transducers the latter. The mechanistic details differ in biology and engineering: animals sense light via chemical excitation from photon absorption, and strain via ion channels that open in response to the physical deformation of membranes or molecules; robots sense light via electrical excitation from photon absorption, and mechanical deformations via strain, magnetic fields, and optics. But both vision and mechanosensation technologies generally transduce sensory cues into analog electrical signals which are subsequently encoded into digital signals.

Since the information provided by a sensor is fundamentally limited by its ability to perceive change in the world, we compare threshold sensitivity, defined as the smallest unit of input that results in a resolved response from the sensor. Both biological and engineered sensors can nearly achieve theoretical limits: single photons and microstrains. For example, biological photoreceptors can resolve individual "quantum bumps" of electrical activity from absorption of single photons (*71*), similar to single-photon avalanche diodes in semiconductors (*72*). The ubiquitous invertebrate campaniform sensilla can detect strains as small as proteins (*73*), whereas hair cells in the mammalian vestibular and auditory system go further still (*74*). But engineered strain gauges can be many orders of magnitude more sensitive (*75*).

Robots generally use a handful of sensors whereas animals have large numbers distributed throughout their bodies. Since redundant distributed sensors can yield richer data more robustly, we compare the number of sensors in each modality. The number of rod and cone cells in a human eye (*74*) is comparable to the number of pixels in the latest smartphones. Invertebrate compound eyes have far fewer individual receptors, with cockroaches having comparable numbers as lidar arrays (*76*). However, animals have many orders of magnitude more strain sensors than robots. Humans, for instance, have roughly two hundred thousand tactile receptors in addition to fifty thousand stretch receptors (*77*, *78*). Insects can have thousands of individual campaniform sensilla to detect exoskeleton strains, thousands of mechanosensitive neurons in chordotonal organs that detect internal strains, and hundreds to thousands of other less well-characterized mechanosensory hairs and sensilla (*79*).

In summary, biological and engineered photoreceptors are comparable in their overall counts and ability to detect visual stimuli. Although engineered mechanoreceptors can detect much smaller stimuli than biological ones (*74*, *75*), biology's ability to integrate staggering numbers of mechanosensors distributed throughout bodies, including the electrical system needed to innervate the sensors, is remarkable. There are robustness advantages to the redundant mechano-sensing streams in animals, as failure of any particular sensor need not halt a runner in its tracks. And the ability to sense throughout the body may also confer advantages for agility, as actionable information may arise in any nook or cranny.

Another potentially interesting comparison is the cost associated with sensing. In animals, neural activity in sensory regions can be substantial (for instance, 8% of resting metabolic rate for the blowfly retina), placing evolutionary pressure on the size and processing of nervous systems (*80*, *81*). However, during movement, metabolic rate increases up to 50-fold (*82*). Taken together, these observations imply that the contribution of sensing to the overall energy budget during running is

low, and therefore is not predictive of overall performance differences, even if they might still be important in the overall fitness of the animal.

Control subsystem performance

The ideal controller for running transmits and transforms sensor and actuator signals to produce versatile behavior. Although animals can walk in the absence of large parts of their nervous systems (*83*) and robots can walk without computers (*84*), electrical control systems are used to run. The physical components and mechanisms differ in biological and engineered control systems: neurons transmit action potentials through axons and synapses using the diffusion of charged molecules; electrical circuits and networks transmit binary or analog signals on wires using electromagnetic waves. Since implementing a control policy requires communication and computation, we consider both in what follows. For the former, we compare axons to network cables; for the latter, we compare natural and artificial spiking neural networks. Larger runners have more time to react to sensor signals before they hit the ground, so we normalize time by the natural period of a runner's limb.

Bandwidth and latency fundamentally limit controller performance (*85*), so we compare both. Many axons can be bundled into a single nerve to increase bandwidth without affecting latency, so we normalize bandwidth by the cross-sectional area of the communication channel. The bandwidth of a standard 10 megabit-per-second Ethernet cable is at least 10,000 times greater than the fastest single axon, but a bundle of 1 million human axons has comparable area-and-period-specific bandwidth (*86*), whereas gigabit Ethernet and other computer network protocols are orders of magnitude faster still. In addition, period-specific latency is at least 1,000 times longer in nerves than an Ethernet cable, and it is impractical for biology to close this gap (*87*). At the smallest scales, buses connecting integrated circuits can have orders-of-magnitude higher bandwidth and lower latency than Ethernet and, thus, even greater advantages over axons.

Effective controllers quickly compute complex policies. The time required for computation in spiking neural networks is proportional to the period-specific latency of a neuron, which time constant is on the order of milliseconds for natural neurons (*88*) and shorter than microseconds for artificial neurons (*89*). However, the number of neurons and synapses differ vastly in natural and artificial networks, with biology outperforming engineering in this metric by orders of magnitude at scales ranging from insects to people. But it is worth remembering that animals rely on their nervous systems to implement a remarkably rich repertoire of behaviors including attracting a mate, finding food, and avoiding predators. It is unclear how much brain is needed for locomotion, as parasitic wasps with fewer than 400 neurons can fly, feed, and find hosts (*90*).

In summary, computer networks vastly exceed the performance of nervous systems in latency and bandwidth of communication and computation, but artificial neural networks are at a substantial disadvantage relative to the size and connectivity of biological networks. Animals cannot practically decrease sensorimotor delay by the orders of magnitude that would be required to compete with robots' communication channels; this fundamental limit surely affects control strategies, for instance by favoring the use of internal models (*87*). Although neuromorphic circuits will continue to increase in complexity, it remains to be seen whether bigger brains are better (*91*) for running and how to make most effective use of the limited brainpower available to robots in the meantime (*92*).

Discussion

Returning to the hypothesis posed at the outset, we found some limited evidence summarized in Fig. 3 that performance differences at the level of subsystems favor biology, partly explaining why animals outrun robots. Fat stores a lot of energy per unit mass, giving animals an advantage in range, particularly compared to robots powered by batteries. Muscle has higher torque density than piezos and motors paired with conventional transmissions, likely conferring some advantage in agility. Although biological sensors are no more sensitive than their engineered counterparts, a large number of them can be distributed throughout the body, lending robustness through redundancy and benefitting agility by providing rich sensor streams from each body part. Finally, brains can theoretically implement much more complex transformations than current integrated circuits due to their vastly greater quantities of neurons and synapses, potentially leading to advantages in range, agility, and robustness. Biological subsystems fare better with respect to robots at insect scales than at human scales, indicating substantial headroom for component performance improvements in roach-sized runners.

However, a simple thought experiment demonstrates that these differences in runner parts do not explain most of the gap in running performance. Suppose we could build cyborg runners using the highest-performing components and subsystems from biological and engineering technologies: a fat-burning, carbon-fibered, muscle-bound monstrosity with distributed sensors and low latency engineered communication channels, all controlled by mind-bogglingly complex spiking neural networks. Would roboticists be able to create cyborgs whose running performance competes with that of animals? This experiment could be carried out in the world of computational simulations, where runner designs are not constrained by the innumerable practical obstacles that make our imagined cyborg physically unrealizable. But even in the most favorable of these worlds, where frames never break and nearly unlimited computational resources control ideal torque sources using perfect state information, we suspect the performance of simulated runners would not approach the agility or robustness of animals in the real world.

If not the performance of subsystems, what is the explanation for why animals can outrun robots? By elimination, the problem must lie with our lack of understanding of how to construct and control a high-performance "whole" using existing high-performance "parts." This is a forgivable shortcoming as at least four fundamental obstacles must be overcome to tackle this integration challenge. First, we lack quantitative metrics for evaluating the many dimensions of running performance, yet these are necessary for improving robot designs using systematic engineering processes. We qualitatively discussed agility and robustness at the outset, but there are only a handful of narrowly-defined ways to measure these properties. Even range, which we conflated with distance, is only well-defined once the runner's behavior and environment are specified. The second and third obstacles are trade-offs and emergence. Stringent tradeoffs potentially arise when subsystems combine since performance of one component might constrain that of another. The opposite is also possible during integration, as emergence is where the behavior of the whole is different than, and irreducible to, the behavior of the parts. The composition of subsystems, especially when feedback is involved, can transform the dynamics for better or worse. These two obstacles are two sides of the same coin in the sense that at their core are unknown but potentially transformative interaction dynamics, and that performing the integration is the only way to expose these dynamics. Yet there are a huge number of ways that the parts can be combined each producing different possibilities for trade-offs and emergent behavior. Unfortunately, the fourth obstacle – the curse of dimensionality *(93, 94)* – admonishes us that these high-dimensional integration spaces cannot be explored by brute force alone. Consequently, it is challenging to find

good mechanical designs in the high-dimensional space of candidate designs, and good control policies in the high-dimensional space of candidate policies.

How can the daunting challenges of integration be overcome? Since tackling the entire system-level problem is daunting, decomposing into subproblems is helpful. Indeed, the conventional "subsystems" we evaluate above are one such decomposition. But performance in these subsystems has been driven by industry's need to efficiently manufacture at scale rather than the roboticist's desire to build the ideal subsystem for running. Instead, we advocate for decomposing into "functional subunits": groupings of parts that reveal the tradeoffs and emergent behavior arising from their integration. As an example, consider the series elastic joint actuator (*95*, *96*): composed of elements of frame, sensing, actuation, and low-level control, its design is subject to the integration challenges and tradeoffs we argue are central to the performance deficit of running robots. At the same time, it features emergent behavior greater than the sum of its parts, as it is torque- and power-dense while maintaining backdrivability and robust force control, simplifying high-level control. The complexity of functional subunits should be more tractable than that of a whole robot, enabling tight integration and performance optimization for their subtasks. They should have reduced and predictable ways of interacting mechanically and electrically with other functional subunits to simplify integration into the broader system. The reduced subset of possibilities ought to make the overall design space more feasible to navigate while still allowing a rich set of runners to explore. As a final note, functional subunit decomposition is compatible with proven tools for building and analyzing runners. For instance, hierarchical models of varying degrees of complexity (*97*, *98*) have revealed how reduced-order emergent behavior is embodied in more complex machines (*99*, *100*) – functional subunits could facilitate this embodiment. And information-based metrics of control architectures like centralization (*101*) and control effort (*102*, *103*) provide potential design criteria at an integrative level applicable to functional subunits and whole robots alike. Although we believe that this approach of decomposing the problem of runner design into functional subunit design will be fruitful, we also understand that it will require creativity, inspiration, and discovery.

Lest roboticists feel sheepish about their machines' performance, we note that biology has a substantial headstart over engineering to explore design and policy spaces. At the lineage level, there have been 1,000 to 10,000,000 times as many generations of animals as robots. Considering population size, there have been one thousand times more humans than robots (of all kinds), and perhaps one quintillion times as many individual insects. In terms of individual experience, animals are less sedentary and have longer lifespans than robots, with ambulatory adult humans taking roughly ten thousand steps per day over decades. In light of these observations, it strikes us that the rate of advancements has been dramatically faster in robots than in animals.

There are several key factors contributing to the disparity between the pace of technological innovation in biology and engineering. Designing and prototyping in engineering is a remarkably rapid and systematic process compared to the undirected search of evolution. Animals must survive to pass on their genes, limiting experimentation from generation-to-generation. And animals in one phylogenetic branch generally cannot benefit from innovations in any other: an adaptation that improves running in a cockroach provides no benefit to a cheetah. In contrast, advancements demonstrated in one robot are readily transferred to others. Furthermore, robots have access to sources of parallelism unavailable to animals: experience can be accumulated on multiple physical and simulated robots simultaneously, and this data can be shared directly. And

these advantages are only limited by the resources invested, for example by the number of researchers in robotics labs, robots on the ground, or servers in the cloud.

We are optimistic that legged robots will someday outrun animals. To hasten this outcome, we conclude by highlighting emerging approaches we regard as potentially-transformative. The bidirectional exchange of principles and approaches between engineering, biology, and physics (*1*, *2*, *4–6*, *92*) has yielded a wonderful constellation of insights and creative designs that have pushed the boundaries of knowledge and possibility. Going forward, systematic comparative studies (rather than single-species inspiration) could reveal generalizable principles for exceptional performance by providing evolutionary context for the factors shaping organisms (*104*). Distributing energy, sensing, actuation, and control throughout robot frames, as animals do, may advance autonomy (*62*, *105*). Bridging the "sim-to-real" gap with better computational models of robot interaction with the environment (*20*, *44*) could dramatically accelerate exploration of design and policy spaces by reducing the number of physical prototypes that need to be built. Bodies can be made easier to control by offloading computation into morphology (*84*, *106*) – this approach remains underdeveloped, but continued advances in material robotics may prove transformative (*62*). Systematically exploring tradeoffs with respect to multiple performance metrics promotes re-use of parts in disparate behaviors (*6*).

The lesson we take from biology is that, although further improvements to components and subsystems are beneficial, the greatest opportunity to improve running robots is to make better use of existing parts. We advocate for integrative exploration of design and policy spaces.

References

1. R. Allen, From feathers to fins: can we understand biological systems—and learn from them? *Bioinspir. Biomim.* **1** (2006).

2. Y. Bar-Cohen, Biomimetics—using nature to inspire human innovation. *Bioinspir. Biomim.* **1**, P1 (2006).

3. A. J. Ijspeert, Biorobotics: Using robots to emulate and investigate agile locomotion. *Science* **346**, 196–203 (2014).

4. N. Gravish, G. V. Lauder, Robotics-inspired biology. *J. Exp. Biol.* **221** (2018).

5. J. Aguilar, T. Zhang, F. Qian, M. Kingsbury, B. McInroe, N. Mazouchova, C. Li, R. Maladen, C. Gong, M. Travers, R. L. Hatton, H. Choset, P. B. Umbanhowar, D. I. Goldman, A review on locomotion robophysics: the study of movement at the intersection of robotics, soft matter and dynamical systems. *Rep. Prog. Phys.* **79**, 110001 (2016).

6. G.-Z. Yang, J. Bellingham, P. E. Dupont, P. Fischer, L. Floridi, R. Full, N. Jacobstein, V. Kumar, M. McNutt, R. Merrifield, B. J. Nelson, B. Scassellati, M. Taddeo, R. Taylor, M. Veloso, Z. L. Wang, R. Wood, The grand challenges of Science Robotics. *Sci Robot* **3** (2018).

7. D. Marr, *Vision: A Computational Approach* (Freeman & Co, 1982).

8. J. D. Wong, J. M. Donelan, Principles of Energetics and Stability in Legged Locomotion. [Preprint] (2019). https://doi.org/10.1007/978-94-007-6046-2_67.

9. C. G. Atkeson, B. Babu, N. Banerjee, D. Berenson, C. P. Bove, X. Cui, M. DeDonato, R. Du, S. Feng, P. Franklin, What Happened at the DARPA Robotics Challenge, and Why? *pdfs.semanticscholar.org* (2016).

10. V. A. Tucker, The energetic cost of moving about. *Am. Sci.* **63**, 413–419 (1975).

11. P. A. Bhounsule, J. Cortell, A. Grewal, B. Hendriksen, J. G. Daniël Karssen, C. Paul, A. Ruina, Low-bandwidth reflex-based control for lower power walking: 65 km on a single battery charge: *Int. J. Rob. Res.* **33**, 1305–1321 (2014).

12. H.-W. Park, P. M. Wensing, S. Kim, High-speed bounding with the MIT Cheetah 2: Control design and experiments. *Int. J. Rob. Res.* **36**, 167–192 (2017).

13. A. T. Baisch, O. Ozcan, B. Goldberg, D. Ithier, R. J. Wood, High speed locomotion for a quadrupedal microrobot. *Int. J. Rob. Res.*, doi: 10.1177/0278364914521473 (2014).

14. J. Hurst, Walk this way: To be useful around people, robots need to learn how to move like we do. *IEEE Spectrum* **56**, 30–51 (2019).

15. D. W. Haldane, R. S. Fearing, Running beyond the bio-inspired regime. *Proceedings - IEEE International Conference on Robotics and Automation* **2015-June**, 4539–4546 (2015).

16. J. R. Usherwood, N. W. Gladman, Why are the fastest runners of intermediate size? Contrasting scaling of mechanical demands and muscle supply of work and power. *Biol. Lett.* **16**, 20200579 (2020).

17. T. Garland, The relation between maximal running speed and body mass in terrestrial mammals. *J. Zool.* **199**, 157–170 (1983).

18. C. J. Clemente, P. J. Bishop, Sticking to the speed limits, *Nature ecology & evolution*. **1** (2017)pp. 1058–1059.

19. T. J. M. Dick, C. J. Clemente, Where Have All the Giants Gone? How Animals Deal with the Problem of Size. *PLoS Biol.* **15**, e2000473 (2017).

20. C. Li, T. Zhang, D. I. Goldman, A Terradynamics of Legged Locomotion on Granular Media. *Science* **339**, 1408–1412 (2013).

21. S. Sponberg, R. J. Full, Neuromechanical response of musculo--skeletal structures in cockroaches during rapid running on rough terrain. *J. Exp. Biol.* **211**, 433–446 (2008).

22. D. W. Haldane, M. M. Plecnik, J. K. Yim, R. S. Fearing, Robotic vertical jumping agility via series-elastic power modulation. *Science Robotics* **1**, eaag2048 (2016).

23. G. Kenneally, A. De, D. E. Koditschek, Design Principles for a Family of Direct-Drive Legged Robots. *IEEE Robotics and Automation Letters* **1**, 900–907 (2016).

24. F. Yu, R. Batke, J. Dao, J. Hurst, K. Green, A. Fern, Dynamic Bipedal Maneuvers through Sim-to-Real Reinforcement Learning, *arXiv [cs.RO]* (2022). http://arxiv.org/abs/2207.07835.

25. A. Hoover, S. A. Burden, X. Fu, S. S. Sastry, R. Fearing, "Bio-inspired design and dynamic maneuverability of a minimally actuated six-legged robot" in *Proceedings of the IEEE International Conference on Biomedical Robotics and Biomechatronics (BIOROB)* (2010; http://dx.doi.org/10.1109/BIOROB.2010.5626034), pp. 869–876.

26. D. L. Jindrich, R. J. Full, Many-legged maneuverability: dynamics of turning in hexapods. *J. Exp. Biol.* **202**, 1603–1623 (1999).

27. M. L. Wynn, C. Clemente, A. F. A. A. Nasir, R. S. Wilson, Running faster causes disaster: trade-offs between speed, manoeuvrability and motor control when running around corners in northern quolls (Dasyurus hallucatus). *J. Exp. Biol.* **218**, 433–439 (2015).

28. T. Haagensen, J. L. Gaschk, J. T. Schultz, C. J. Clemente, Exploring the limits to turning performance with size and shape variation in dogs. *J. Exp. Biol.* **225** (2022).

29. H. Tan, A. M. Wilson, Grip and limb force limits to turning performance in competition horses. *Proc. Biol. Sci.* **278**, 2105–2111 (2011).

30. A. M. Wilson, J. C. Lowe, K. Roskilly, P. E. Hudson, K. A. Golabek, J. W. McNutt, Locomotion dynamics of hunting in wild cheetahs. *Nature* **498**, 185–189 (2013).

31. R. M. Walter, Kinematics of 90 degrees running turns in wild mice. *J. Exp. Biol.* **206**, 1739–1749 (2003).

32. K. Sreenath, H.-W. Park, I. Poulakakis, J. W. Grizzle, A Compliant Hybrid Zero Dynamics Controller for Stable, Efficient and Fast Bipedal Walking on MABEL. *Int. J. Rob. Res.* **30**, 1170–1193 (2011).

33. D. L. Jindrich, R. J. Full, Dynamic stabilization of rapid hexapedal locomotion. *J. Exp. Biol.* **205**, 2803–2823 (2002).

34. A. Brandwood, A. S. Jayes, R. M. Alexander, Incidence of healed fracture in the skeletons of birds, molluscs and primates. *J. Zool.* **208**, 55–62 (1986).

35. Z. Emberts, I. Escalante, P. W. Bateman, The ecology and evolution of autotomy. *Biol. Rev. Camb. Philos. Soc.* **94**, 1881–1896 (2019).

36. C. Guffey, Leg Autotomy and Its Potential Fitness Costs for Two Species of Harvestmen (Arachnida, Opiliones). *J. Arachnol.* **26**, 296–302 (1998).

37. J. Lee, J. Hwangbo, L. Wellhausen, V. Koltun, M. Hutter, Learning quadrupedal locomotion over challenging terrain. *Sci Robot* **5** (2020).

38. J. P. Olberding, L. D. McBrayer, T. E. Higham, Performance and three-dimensional kinematics of bipedal lizards during obstacle negotiation. *J. Exp. Biol.* **215**, 247–255 (2012).

39. M. A. Daley, J. R. Usherwood, G. Felix, A. A. Biewener, Running over rough terrain: guinea fowl maintain dynamic stability despite a large unexpected change in substrate height. *J. Exp. Biol.* **209**, 171–187 (2006).

40. A. V. Birn-Jeffery, C. M. Hubicki, Y. Blum, D. Renjewski, J. W. Hurst, M. A. Daley, Don't break a leg: running birds from quail to ostrich prioritise leg safety and economy on uneven terrain. *J. Exp. Biol.* **217**, 3786–3796 (2014).

41. T. Kohlsdorf, A. A. Biewener, Negotiating obstacles: running kinematics of the lizard Sceloporus malachiticus. *J. Zool.* **270**, 359–371 (2006).

42. K. Jayaram, R. J. Full, Cockroaches traverse crevices, crawl rapidly in confined spaces, and inspire a soft, legged robot. *Proc. Natl. Acad. Sci. U. S. A.* **113**, E950–7 (2016).

43. C. Li, A. O. Pullin, D. W. Haldane, H. K. Lam, R. S. Fearing, R. J. Full, Terradynamically streamlined shapes in animals and robots enhance traversability through densely cluttered terrain. *Bioinspir. Biomim.* **10**, 046003 (2015).

44. C. Li, P. B. Umbanhowar, H. Komsuoglu, D. E. Koditschek, D. I. Goldman, Sensitive dependence of the motion of a legged robot on granular media. *Proc. Natl. Acad. Sci. U. S. A.* **106**, 3029–3034 (2009).

45. R. Riener, L. Rabezzana, Y. Zimmermann, Do Robots Outperform Humans in Human-Centered Domains? *Frontiers in Robotics and AI* **10** (2023).

46. N. P. Smith, C. J. Barclay, D. S. Loiselle, The efficiency of muscle contraction. *Prog. Biophys. Mol. Biol.* **88**, 1–58 (2005).

47. D. Dunn-Rankin, E. M. Leal, D. C. Walther, Personal power systems. *Prog. Energy Combust. Sci.* **31**, 422–465 (2005).

48. M. Wishnofsky, Caloric equivalents of gained or lost weight. *Am. J. Clin. Nutr.* **6**, 542–546 (1958).

49. M. Raibert, K. Blankespoor, G. Nelson, R. Playter, Bigdog, the rough–terrain quadruped robot. 10823–10825 (2008).

50. C. R. Taylor, Structural and functional limits to oxidative metabolism: insights from scaling. *Annu. Rev. Physiol.* **49**, 135–146 (1987).

51. M. Günther, R. Rockenfeller, T. Weihmann, D. F. B. Haeufle, T. Götz, S. Schmitt, Rules of nature's Formula Run: Muscle mechanics during late stance is the key to explaining maximum running speed. *J. Theor. Biol.* **523**, 110714 (2021).

52. M. R. Hirt, W. Jetz, B. C. Rall, U. Brose, A general scaling law reveals why the largest animals are not the fastest. *Nat Ecol Evol* **1**, 1116–1122 (2017).

53. C. Thurber, L. R. Dugas, C. Ocobock, B. Carlson, J. R. Speakman, H. Pontzer, Extreme events reveal an alimentary limit on sustained maximal human energy expenditure. *Science Advances* **5**, eaaw0341 (2019).

54. G. Girishkumar, B. McCloskey, A. C. Luntz, S. Swanson, W. Wilcke, Lithium−Air Battery: Promise and Challenges. *J. Phys. Chem. Lett.* **1**, 2193–2203 (2010).

55. J. F. V. Vincent, U. G. K. Wegst, Design and mechanical properties of insect cuticle. *Arthropod Struct. Dev.* **33**, 187–199 (2004).

56. A. A. Biewener, Biomechanics of mammalian terrestrial locomotion. *Science* **250**, 1097–1103 (1990).

57. M. F. Ashby, D. Cebon, Materials selection in mechanical design. *Le Journal de Physique IV* **03**, C7–1–C7–9 (1993).

58. S. O. Andersen, T. Weis-Fogh, "Resilin. A Rubberlike Protein in Arthropod Cuticle" in *Advances in Insect Physiology*, J. W. L. Beament, J. E. Treherne, V. B. Wigglesworth, Eds. (Academic Press, 1964; https://www.sciencedirect.com/science/article/pii/S0065280608600715)vol. 2, pp. 1–65.

59. C. M. Pollock, R. E. Shadwick, Relationship between body mass and biomechanical properties of limb tendons in adult mammals. *Am. J. Physiol.* **266**, R1016–21 (1994).

60. D. J. Hyun, S. Seok, J. Lee, S. Kim, High speed trot-running: Implementation of a hierarchical controller using proprioceptive impedance control on the MIT Cheetah. *Int. J. Rob. Res.* **33**, 1417–1445 (2014).

61. S. E. Naleway, M. M. Porter, J. McKittrick, M. A. Meyers, Structural Design Elements in Biological Materials: Application to Bioinspiration. *Adv. Mater.* **27**, 5455–5476 (2015).

62. M. A. McEvoy, N. Correll, Materials that couple sensing, actuation, computation, and communication. *Science* **347**, 1261689 (2015).

63. J. Wang, D. Gao, P. S. Lee, Recent Progress in Artificial Muscles for Interactive Soft Robotics. *Adv. Mater.* **33**, e2003088 (2021).

64. L. Ricotti, B. Trimmer, A. W. Feinberg, R. Raman, K. K. Parker, R. Bashir, M. Sitti, S. Martel, P. Dario, A. Menciassi, Biohybrid actuators for robotics: A review of devices actuated by living cells. *Sci Robot* **2** (2017).

65. M. Hutter, C. Gehring, M. Bloesch, M. A. Hoepflinger, C. D. Remy, R. Siegwart, "StarlETH: A compliant quadrupedal robot for fast, efficient, and versatile locomotion" in *Adaptive Mobile Robotics* (WORLD SCIENTIFIC, 2012; https://doi.org/10.1142/9789814415958_0062), pp. 483–490.

66. N. Paine, S. Oh, L. Sentis, Design and Control Considerations for High-Performance Series Elastic Actuators. *IEEE/ASME Trans. Mechatron.* **19**, 1080–1091 (2014).

67. X. Zhou, S. Bi, A survey of bio-inspired compliant legged robot designs. *Bioinspir. Biomim.* **7**, 041001 (2012).

68. S. J. Longo, S. M. Cox, E. Azizi, M. Ilton, J. P. Olberding, R. St Pierre, S. N. Patek, Beyond power amplification: latch-mediated spring actuation is an emerging framework for the study of diverse elastic systems. [Preprint] (2019). https://doi.org/10.1242/jeb.197889.

69. N. A. Curtin, H. L. A. Bartlam-Brooks, T. Y. Hubel, J. C. Lowe, A. R. Gardner-Medwin, E. Bennitt, S. J. Amos, M. Lorenc, T. G. West, A. M. Wilson, Remarkable muscles, remarkable locomotion in desert-dwelling wildebeest. *Nature* **563**, 393–396 (2018).

70. S. Soatto, "Actionable Information in Vision" in *Machine Learning for Computer Vision*, R. Cipolla, S. Battiato, G. M. Farinella, Eds. (Springer Berlin / Heidelberg, 2013; http://dx.doi.org/10.1007/978-3-642-28661-2_2)vol. 411 of *Studies in Computational Intelligence*, pp. 17–48.

71. E. Warrant, M. Dacke, Vision and visual navigation in nocturnal insects. *Annu. Rev. Entomol.* **56**, 239–254 (2011).

72. S. Cova, M. Ghioni, A. Lacaita, C. Samori, F. Zappa, Avalanche photodiodes and quenching circuits for single-photon detection. *Appl. Opt.* **35**, 1956–1976 (1996).

73. G. F. Dinges, T. Bockemühl, F. Iacoviello, P. R. Shearing, A. Büschges, A. Blanke, Ultra high-resolution biomechanics suggest that substructures within insect mechanosensors decisively affect their sensitivity. *J. R. Soc. Interface* **19**, 20220102 (2022).

74. D. Purves, G. J. Augustine, D. Fitzpatrick, L. C. Katz, A.-S. LaMantia, J. O. McNamara, S. Mark Williams, Eds., *Neuroscience* (Sinauer Associates, 2001).

75. G. Gautschi, *Piezoelectric Sensorics* (Springer Berlin Heidelberg, 2002; https://link.springer.com/book/10.1007/978-3-662-04732-3).

76. J. J. Wolken, P. D. Gupta, Photoreceptor structures. The retinal cells of the cockroach eye. IV. Periplaneta americana and Blaberus giganteus. *J. Biophys. Biochem. Cytol.* **9**, 720–724 (1961).

77. G. Corniani, H. P. Saal, Tactile innervation densities across the whole body. *J. Neurophysiol.* **124**, 1229–1240 (2020).

78. R. W. Banks, D. Barker, *Myology: Basic and Clinical* (McGraw-Hill, 2004).

79. J. C. Tuthill, R. I. Wilson, Mechanosensation and Adaptive Motor Control in Insects. *Curr. Biol.* **26**, R1022–R1038 (2016).

80. J. E. Niven, J. C. Anderson, S. B. Laughlin, Fly photoreceptors demonstrate energy-information trade-offs in neural coding. *PLoS Biol.* **5**, e116 (2007).

81. J. E. Niven, S. B. Laughlin, Energy limitation as a selective pressure on the evolution of sensory systems. *J. Exp. Biol.* **211**, 1792–1804 (2008).

82. E. R. Weibel, L. D. Bacigalupe, B. Schmitt, H. Hoppeler, Allometric scaling of maximal metabolic rate in mammals: Muscle aerobic capacity as determinant factor. *Respir. Physiol. Neurobiol.* **140**, 115–132 (2004).

83. M. L. Shik, G. N. Orlovsky, Neurophysiology of locomotor automatism. *Physiol. Rev.* **56**, 465–501 (1976).

84. T. McGeer, Passive dynamic walking. *Int. J. Rob. Res.* **9**, 62 (1990).

85. G. N. Nair, F. Fagnani, S. Zampieri, R. J. Evans, Feedback Control Under Data Rate Constraints: An Overview. *Proc. IEEE* **95**, 108–137 (2007).

86. K. Koch, J. McLean, R. Segev, M. A. Freed, M. J. Berry 2nd, V. Balasubramanian, P. Sterling, How much the eye tells the brain. *Curr. Biol.* **16**, 1428–1434 (2006).

87. H. L. More, J. M. Donelan, Scaling of sensorimotor delays in terrestrial mammals. *Proc. Biol. Sci.* **285** (2018).

88. J. J. Hopfield, D. W. Tank, "Neural" computation of decisions in optimization problems. *Biol. Cybern.* **52**, 141–152 (1985).

89. J. Pei, L. Deng, S. Song, M. Zhao, Y. Zhang, S. Wu, G. Wang, Z. Zou, Z. Wu, W. He, F. Chen, N. Deng, S. Wu, Y. Wang, Y. Wu, Z. Yang, C. Ma, G. Li, W. Han, H. Li, H. Wu, R. Zhao, Y. Xie, L. Shi, Towards artificial general intelligence with hybrid Tianjic chip architecture. *Nature* **572**, 106–111 (2019).

90. A. A. Polilov, The smallest insects evolve anucleate neurons. *Arthropod Struct. Dev.* **41**, 29–34 (2012).

91. L. Chittka, J. Niven, Are Bigger Brains Better? *Curr. Biol.* **19**, R995–R1008 (2009).

92. G. C. H. E. de Croon, J. J. G. Dupeyroux, S. B. Fuller, J. A. R. Marshall, Insect-inspired AI for autonomous robots. *Sci. Robot.* **7** (2022).

93. R. Bellman, *Dynamic Programming* (Princeton University Press, 1957; http://books.google.com/books?id=wdtoPwAACAAJ).

94. N. A. Bernstein, *The Co-Ordination and Regulation of Movements* (Pergamon Press Ltd., 1967).

95. G. A. Pratt, M. M. Williamson, "Series elastic actuators" in *Proceedings 1995 IEEE/RSJ International Conference on Intelligent Robots and Systems. Human Robot Interaction and Cooperative Robots* (ieeexplore.ieee.org, 1995; http://dx.doi.org/10.1109/IROS.1995.525827)vol. 1, pp. 399–406 vol.1.

96. J. E. Pratt, B. T. Krupp, "Series Elastic Actuators for legged robots" in *Unmanned Ground Vehicle Technology VI* (International Society for Optics and Photonics, 2004; https://www.spiedigitallibrary.org/conference-proceedings-of-spie/5422/0000/Series-Elastic-Actuators-for-legged-robots/10.1117/12.548000.short)vol. 5422, pp. 135–145.

97. P. Holmes, R. J. Full, D. E. Koditschek, J. Guckenheimer, The Dynamics of Legged Locomotion: Models, Analyses, and Challenges. *SIAM Rev.* **48**, 207–304 (2006).

98. R. J. Full, D. E. Koditschek, Templates and anchors: neuromechanical hypotheses of legged locomotion on land. *J. Exp. Biol.* **202**, 3325–3332 (1999).

99. R. Blickhan, A. Seyfarth, H. Geyer, S. Grimmer, H. Wagner, M. Günther, Intelligence by mechanics. *Philos. Trans. A Math. Phys. Eng. Sci.* **365**, 199–220 (2007).

100. J. R. Walter, M. Günther, D. F. B. Haeufle, S. Schmitt, A geometry- and muscle-based control architecture for synthesising biological movement. *Biol. Cybern.* **115**, 7–37 (2021).

101. I. D. Neveln, A. Tirumalai, S. Sponberg, Information-based centralization of locomotion in animals and robots. *Nat. Commun.* **10**, 3655 (2019).

102. D. F. B. Haeufle, M. Günther, G. Wunner, S. Schmitt, Quantifying control effort of biological and technical movements: An information-entropy-based approach. *Phys. Rev. E* **89**, 1–7 (2014).

103. D. F. B. Haeufle, I. Wochner, D. Holzmüller, D. Driess, M. Günther, S. Schmitt, Muscles Reduce Neuronal Information Load: Quantification of Control Effort in Biological vs. Robotic Pointing and Walking. *Front Robot AI* **7**, 77 (2020).

104. N. Jourjine, H. E. Hoekstra, Expanding evolutionary neuroscience: insights from comparing variation in behavior. *Neuron* **109**, 1084–1099 (2021).

105. C. A. Aubin, B. Gorissen, E. Milana, P. R. Buskohl, N. Lazarus, G. A. Slipher, C. Keplinger, J. Bongard, F. Iida, J. A. Lewis, R. F. Shepherd, Towards enduring autonomous

robots via embodied energy. *Nature* **602**, 393–402 (2022).

106. C. Paul, Morphological computation: A basis for the analysis of morphology and control requirements. *Rob. Auton. Syst.* **54**, 619–630 (2006).

107. G. B. West, W. H. Woodruff, J. H. Brown, Allometric scaling of metabolic rate from molecules and mitochondria to cells and mammals. *Proc. Natl. Acad. Sci. U. S. A.* **99 Suppl 1**, 2473–2478 (2002).

108. W. G. Eberhard, W. T. Wcislo, "Grade Changes in Brain–Body Allometry: Morphological and Behavioural Correlates of Brain Size in Miniature Spiders, Insects and Other Invertebrates" in *Advances in Insect Physiology*, J. Casas, Ed. (Academic Press, 2011; http://www.sciencedirect.com/science/article/pii/B9780123876683000040)vol. 40, pp. 155–214.

109. R. Franz, J. Hummel, E. Kienzle, P. Kölle, H.-C. Gunga, M. Clauss, Allometry of visceral organs in living amniotes and its implications for sauropod dinosaurs. *Proc. Biol. Sci.* **276**, 1731–1736 (2009).

110. I. J. Gordon, A. W. Illius, The functional significance of the browser-grazer dichotomy in African ruminants. *Oecologia* **98**, 167–175 (1994).

111. S. L. Lindstedt, M. S. Boyce, Seasonality, Fasting Endurance, and Body Size in Mammals. *Am. Nat.* **125**, 873–878 (1985).

112. S. M. O'Regan, C. G. Guglielmo, G. M. Taylor, Measurement of arthropod body composition using quantitative magnetic resonance. *Invertebr. Biol.* **131**, 216–223 (2012).

113. M. H. Raibert, K. Blankespoor, G. Nelson, R. Playter, the BigDog Team, BigDog, the Rough--Terrain Quadruped Robot. *Proceedings of the IFAC World Congress*, 10822–10825 (2008).

114. S. Seok, A. Wang, M. Y. (michael) Chuah, D. J. Hyun, J. Lee, D. M. Otten, J. H. Lang, S. Kim, Design Principles for Energy-Efficient Legged Locomotion and Implementation on the MIT Cheetah Robot. *IEEE/ASME Trans. Mechatron.* **20**, 1117–1129 (2015).

115. G. Bledt, M. J. Powell, B. Katz, J. Di Carlo, P. M. Wensing, S. Kim, "MIT Cheetah 3: Design and Control of a Robust, Dynamic Quadruped Robot" in *2018 IEEE/RSJ International Conference on Intelligent Robots and Systems (IROS)* (2018; http://dx.doi.org/10.1109/IROS.2018.8593885), pp. 2245–2252.

116. M. Hutter, C. Gehring, M. A. Höpflinger, M. Blösch, R. Siegwart, Toward Combining Speed, Efficiency, Versatility, and Robustness in an Autonomous Quadruped. *IEEE Trans. Rob.* **30**, 1427–1440 (2014).

117. M. Hutter, C. Gehring, D. Jud, A. Lauber, C. D. Bellicoso, V. Tsounis, J. Hwangbo, K. Bodie, P. Fankhauser, M. Bloesch, R. Diethelm, S. Bachmann, A. Melzer, M. Hoepflinger, "ANYmal - a highly mobile and dynamic quadrupedal robot" in *2016 IEEE/RSJ International Conference on Intelligent Robots and Systems (IROS)* (2016;

http://dx.doi.org/10.1109/IROS.2016.7758092), pp. 38–44.

118. K. D. Hall, What is the required energy deficit per unit weight loss? *Int. J. Obes.* **32**, 573–576 (2008).

119. B. D. McCloskey, Expanding the Ragone Plot: Pushing the Limits of Energy Storage. *J. Phys. Chem. Lett.* **6**, 3592–3593 (2015).

120. R. K. Suarez, J. R. Lighton, G. S. Brown, O. Mathieu-Costello, Mitochondrial respiration in hummingbird flight muscles. *Proc. Natl. Acad. Sci. U. S. A.* **88**, 4870–4873 (1991).

121. J. M. Brockway, Derivation of formulae used to calculate energy expenditure in man. *Hum. Nutr. Clin. Nutr.* **41**, 463–471 (1987).

122. V. M. Savage, J. F. Gillooly, W. H. Woodruff, G. B. West, A. P. Allen, B. J. Enquist, J. H. Brown, The predominance of quarter-power scaling in biology. *Funct. Ecol.* **18**, 257–282 (2004).

123. K. A. Hammond, J. Diamond, Maximal sustained energy budgets in humans and animals. *Nature* **386**, 457–462 (1997).

124. M. H. Dickinson, C. T. Farley, R. J. Full, M. A. R. Koehl, R. Kram, S. Lehman, How Animals Move: An Integrative View. *Science* **288**, 100–106 (2000).

125. D. M. Bramble, D. E. Lieberman, Endurance running and the evolution of Homo. *Nature* **432**, 345–352 (2004).

126. M. Ilton, M. S. Bhamla, X. Ma, S. M. Cox, L. L. Fitchett, Y. Kim, J.-S. Koh, D. Krishnamurthy, C.-Y. Kuo, F. Z. Temel, A. J. Crosby, M. Prakash, G. P. Sutton, R. J. Wood, E. Azizi, S. Bergbreiter, S. N. Patek, The principles of cascading power limits in small, fast biological and engineered systems. *Science* **360** (2018).

127. M. F. Ashby, *Materials Selection in Mechanical Design* (Butterworth-Heinemann, 1992; https://play.google.com/store/books/details?id=k0l1lAEACAAJ).

128. R. J. Wootton, Invertebrate paraxial locomotory appendages: Design, deformation and control. *J. Exp. Biol.* **202**, 3333–3345 (1999).

129. J.-H. Dirks, E. Parle, D. Taylor, Fatigue of insect cuticle. *J. Exp. Biol.*, doi: 10.1242/jeb.083824 (2013).

130. S. R. Bullimore, J. F. Burn, Scaling of elastic energy storage in mammalian limb tendons: do small mammals really lose out? *Biol. Lett.* **1**, 57–59 (2005).

131. A. Biewener, R. Baudinette, In vivo muscle force and elastic energy storage during steady-speed hopping of tammar wallabies (Macropus eugenii). *J. Exp. Biol.* **198**, 1829–1841 (1995).

132. G. A. Pratt, Legged robots at MIT: What's new since Raibert. *IEEE Robot. Autom. Mag.*

7, 15–19 (2000).

133. K. C. Galloway, J. E. Clark, D. E. Koditschek, Variable Stiffness Legs for Robust, Efficient, and Stable Dynamic Running. *J. Mech. Robot.* **5**, 011009 (2013).

134. O. Ozcan, A. T. Baisch, D. Ithier, R. J. Wood, Powertrain selection for a biologically-inspired miniature quadruped robot. *Proceedings - IEEE International Conference on Robotics and Automation*, 2398–2405 (2014).

135. S. Kim, P. M. Wensing, Design of Dynamic Legged Robots. *Foundations and Trends® in Robotics* **5**, 117–190 (2017).

136. S. B. Williams, A. M. Wilson, L. Rhodes, J. Andrews, R. C. Payne, Functional anatomy and muscle moment arms of the pelvic limb of an elite sprinting athlete: the racing greyhound (Canis familiaris). *J. Anat.* **213**, 361–372 (2008).

137. R. Full, A. Ahn, Static forces and moments generated in the insect leg: comparison of a three-dimensional musculo-skeletal computer model with experimental measurements. *J. Exp. Biol.* **198**, 1285–1298 (1995).

138. C. N. Maganaris, V. Baltzopoulos, D. Tsaopoulos, Muscle fibre length-to-moment arm ratios in the human lower limb determined in vivo. *J. Biomech.* **39**, 1663–1668 (2006).

139. a. N. Ahn, R. J. Full, A motor and a brake: two leg extensor muscles acting at the same joint manage energy differently in a running insect. *J. Exp. Biol.* **205**, 379–389 (2002).

140. T. Siebert, T. Weihmann, C. Rode, R. Blickhan, Cupiennius salei: biomechanical properties of the tibia-metatarsus joint and its flexing muscles. *J. Comp. Physiol. B* **180**, 199–209 (2010).

141. K. R. S. Holzbaur, S. L. Delp, G. E. Gold, W. M. Murray, Moment-generating capacity of upper limb muscles in healthy adults. *J. Biomech.* **40**, 2442–2449 (2007).

142. J. R. Baxter, S. J. Piazza, Plantar flexor moment arm and muscle volume predict torque-generating capacity in young men. *J. Appl. Physiol.* **116**, 538–544 (2014).

143. P. M. Wensing, A. Wang, S. Member, S. Seok, D. Otten, J. Lang, S. Kim, Proprioceptive Actuator Design in the MIT Cheetah : Impact Mitigation and High-Bandwidth Physical Interaction for Dynamic Legged Robots. **33**, 509–522 (2017).

144. S. Wolf, O. Eiberger, G. Hirzinger, "The DLR FSJ: Energy based design of a variable stiffness joint" in *2011 IEEE International Conference on Robotics and Automation* (2011; http://dx.doi.org/10.1109/ICRA.2011.5980303), pp. 5082–5089.

145. Q. Hua, W. Zhou, S. Zhu, Y. Yao, C. Cheng, A. Xie, D. Zhang, Design of a High-torque Robot Joint and Its Control System. *J. Phys. Conf. Ser.* **2281**, 012007 (2022).

146. M. E. Carney, T. Shu, R. Stolyarov, J.-F. Duval, H. M. Herr, Design and Preliminary Results of a Reaction Force Series Elastic Actuator for Bionic Knee and Ankle Prostheses.

IEEE Transactions on Medical Robotics and Bionics **3**, 542–553 (2021).

147. K. Jayaram, J. Shum, S. Castellanos, E. Farrell Helbling, R. J. Wood, Scaling down an insect-size microrobot, HAMR-VI into HAMR-Jr, *arXiv [cs.RO]* (2020). http://arxiv.org/abs/2003.03337.

148. N. Doshi, B. Goldberg, R. Sahai, N. Jafferis, D. Aukes, R. J. Wood, J. A. Paulson, "Model driven design for flexure-based Microrobots" in *2015 IEEE/RSJ International Conference on Intelligent Robots and Systems (IROS)* (2015; http://dx.doi.org/10.1109/IROS.2015.7353959), pp. 4119–4126.

149. R. Josephson, Contraction Dynamics and Power Output of Skeletal Muscle. *Annu. Rev. Physiol.* **55**, 527–546 (1993).

150. R. J. Full, K. Meijer, "Artificial muscles versus natural actuators from frogs to flies" in *Smart Structures and Materials 2000: Electroactive Polymer Actuators and Devices (EAPAD)* (SPIE, 2000; https://www.spiedigitallibrary.org/conference-proceedings-of-spie/3987/0000/Artificial-muscles-versus-natural-actuators-from-frogs-to-flies/10.1117/12.387761.short)vol. 3987, pp. 2–9.

151. G. N. Askew, R. L. Marsh, Muscle designed for maximum short-term power output: quail flight muscle. *J. Exp. Biol.* **205**, 2153–2160 (2002).

152. R. S. James, J. D. Altringham, D. F. Goldspink, The mechanical properties of fast and slow skeletal muscles of the mouse in relation to their locomotory function. *J. Exp. Biol.* **198**, 491–502 (1995).

153. R. S. James, R. S. Wilson, Explosive jumping: extreme morphological and physiological specializations of Australian rocket frogs (Litoria nasuta). *Physiol. Biochem. Zool.* **81**, 176–185 (2008).

154. T. J. Roberts, J. A. Scales, Mechanical power output during running accelerations in wild turkeys. *J. Exp. Biol.* **205**, 1485–1494 (2002).

155. B. D. O. Anderson, Adaptive systems, lack of persistency of excitation and bursting phenomena. *Automatica* **21**, 247–258 (1985).

156. K. Jayaram, J. Shum, S. Castellanos, E. F. Helbling, R. J. Wood, "Scaling down an insect-size microrobot, HAMR-VI into HAMR-Jr" in *2020 IEEE International Conference on Robotics and Automation (ICRA)* (2020; http://dx.doi.org/10.1109/ICRA40945.2020.9197436), pp. 10305–10311.

157. D. Purves, G. J. Augustine, D. Fitzpatrick, W. Hall C., A.-S. LaMantia, R. D. Mooney, M. L. Platt, L. E. White, Eds., *Neuroscience* (Sinauer Associates, Publishers, Sunderland, Mass, 3rd ed., 2004).

158. F. Jaramillo, K. Wiesenfeld, Mechanoelectrical transduction assisted by Brownian motion: a role for noise in the auditory system. *Nat. Neurosci.* **1**, 384–388 (1998).

159. G. Gautschi, *Piezoelectric Sensorics: Force Strain Pressure Acceleration And Acoustic Emission Sensors Materials and Amplifiers* (Springer Science & Business Media, 2006).

160. E. Warrant, M. Dacke, Vision and visual navigation in nocturnal insects. *Annual Review of Entomology, Vol 57* **56**, 239–254 (2011).

161. R. Cagan, Principles of Drosophila eye differentiation. *Curr. Top. Dev. Biol.* **89**, 115–135 (2009).

162. P. Pirih, M. Ilić, J. Rudolf, K. Arikawa, D. G. Stavenga, G. Belušič, The giant butterfly-moth Paysandisia archon has spectrally rich apposition eyes with unique light-dependent photoreceptor dynamics. *J. Comp. Physiol. A Neuroethol. Sens. Neural Behav. Physiol.* **204**, 639–651 (2018).

163. A. A. Makarova, V. B. Meyer-Rochow, A. A. Polilov, Morphology and scaling of compound eyes in the smallest beetles (Coleoptera: Ptiliidae). *Arthropod Struct. Dev.* **48**, 83–97 (2019).

164. A. Engel, C. Franzini-Armstrong, *Myology: Basic And Clinical* (McGraw-Hill, ed. 3, 2005).

165. A. Honkanen, A. Adden, J. Da Silva Freitas, S. Heinze, The insect central complex and the neural basis of navigational strategies. *J. Exp. Biol.* **222**, jeb188854 (2019).

166. J. C. Tuthill, E. Azim, Proprioception. *Curr. Biol.* **28**, R194–R203 (2018).

167. P. Cordo, V. S. Gurfinkel, L. Bevan, G. K. Kerr, Proprioceptive consequences of tendon vibration during movement. *J. Neurophysiol.* **74**, 1675–1688 (1995).

168. K. L. Page, T. Matheson, Functional recovery of aimed scratching movements after a graded proprioceptive manipulation. *J. Neurosci.* **29**, 3897–3907 (2009).

169. S. N. Mohamed Thangal, J. M. Donelan, Scaling of inertial delays in terrestrial mammals. *PLoS One* **15**, e0217188 (2020).

170. D. M. MacKay, W. S. McCulloch, The limiting information capacity of a neuronal link. *Bull. Math. Biophys.* **14**, 127–135 (1952).

171. A. Borst, F. E. F. E. Theunissen, Information theory and neural coding. *Nat. Neurosci.* **2**, 947–957 (1999).

172. Beckhoff Automation, "EtherCAT System Documentation" (2018); https://download.beckhoff.com/download/document/io/ethercat-terminals/ethercatsystem_en.pdf.

173. InfiniBand Trade Association, InfiniBand (2020). https://www.infinibandta.org/.

174. J. a. Perge, J. E. Niven, E. Mugnaini, V. Balasubramanian, P. Sterling, Why Do Axons Differ in Caliber? *J. Neurosci.* **32**, 626–638 (2012).

175. J. A. Perge, K. Koch, R. Miller, P. Sterling, V. Balasubramanian, How the optic nerve allocates space, energy capacity, and information. *J. Neurosci.* **29**, 7917–7928 (2009).

176. A. A. Faisal, J. A. White, S. B. Laughlin, Ion-channel noise places limits on the miniaturization of the brain's wiring. *Curr. Biol.* **15**, 1143–1149 (2005).

177. M. Vaiman, R. Abuita, I. Bekerman, Optic nerve sheath diameters in healthy adults measured by computer tomography. *Int. J. Ophthalmol.* **8**, 1240–1244 (2015).

178. H. L. More, "Scaling of sensorimotor control in terrestrial mammals," thesis, Simon Fraser University (2013).

179. I. A. Boyd, K. U. Kalu, Scaling factor relating conduction velocity and diameter for myelinated afferent nerve fibres in the cat hind limb. *J. Physiol.* **289**, 277–297 (1979).

180. H. L. More, J. R. Hutchinson, D. F. Collins, D. J. Weber, S. K. H. Aung, J. M. Donelan, Scaling of sensorimotor control in terrestrial mammals. *Proceedings of the Royal Society B: Biological Sciences* **277**, 3563–3568 (2010).

181. K. G. Pearson, R. B. Stein, S. K. Malhotra, Properties of action potentials from insect motor nerve fibres. *J. Exp. Biol.* **53**, 299–316 (1970).

182. S. Greengard, Neuromorphic chips take shape. *Commun. ACM* **63**, 9–11 (2020).

183. W. Zhang, B. Gao, J. Tang, P. Yao, S. Yu, M.-F. Chang, H.-J. Yoo, H. Qian, H. Wu, Neuro-inspired computing chips. *Nature Electronics* **3**, 371–382 (2020).

184. T. Yamazaki, J. Igarashi, H. Yamaura, Human-scale Brain Simulation via Supercomputer: A Case Study on the Cerebellum. *Neuroscience* **462**, 235–246 (2021).

185. F. Scarselli, A. Chung Tsoi, Universal Approximation Using Feedforward Neural Networks: A Survey of Some Existing Methods, and Some New Results. *Neural Netw.* **11**, 15–37 (1998).

186. Y. LeCun, Y. Bengio, G. Hinton, Deep learning. *Nature* **521**, 436–444 (2015).

187. P. A. Merolla, J. V. Arthur, R. Alvarez-Icaza, A. S. Cassidy, J. Sawada, F. Akopyan, B. L. Jackson, N. Imam, C. Guo, Y. Nakamura, B. Brezzo, I. Vo, S. K. Esser, R. Appuswamy, B. Taba, A. Amir, M. D. Flickner, W. P. Risk, R. Manohar, D. S. Modha, Artificial brains. A million spiking-neuron integrated circuit with a scalable communication network and interface. *Science* **345**, 668–673 (2014).

188. C.-K. Lin, A. Wild, G. N. Chinya, Y. Cao, M. Davies, D. M. Lavery, H. Wang, Programming spiking neural networks on Intel's loihi. *Computer* **51**, 52–61 (2018).

189. M. V. DeBole, B. Taba, A. Amir, F. Akopyan, A. Andreopoulos, W. P. Risk, J. Kusnitz, C. Ortega Otero, T. K. Nayak, R. Appuswamy, P. J. Carlson, A. S. Cassidy, P. Datta, S. K. Esser, G. J. Garreau, K. L. Holland, S. Lekuch, M. Mastro, J. McKinstry, C. di Nolfo, B. Paulovicks, J. Sawada, K. Schleupen, B. G. Shaw, J. L. Klamo, M. D. Flickner, J. V.

Arthur, D. S. Modha, TrueNorth: Accelerating From Zero to 64 Million Neurons in 10 Years. *Computer* **52**, 20–29 (2019).

190. M. Davies, A. Wild, G. Orchard, Y. Sandamirskaya, G. A. F. Guerra, P. Joshi, P. Plank, S. R. Risbud, Advancing Neuromorphic Computing With Loihi: A Survey of Results and Outlook. *Proc. IEEE* **109**, 911–934 (2021).

191. A. S. Chiang, Y. C. Liu, S. L. Chiu, S. H. Hu, C. Y. Huang, C. H. Hsieh, Three-dimensional mapping of brain neuropils in the cockroach, Diploptera punctata. *J. Comp. Neurol.* **440**, 1–11 (2001).

192. J. Sallet, R. B. Mars, M. P. Noonan, J. L. Andersson, J. X. O'Reilly, S. Jbabdi, P. L. Croxson, M. Jenkinson, K. L. Miller, M. F. S. Rushworth, Social network size affects neural circuits in macaques. *Science* **334**, 697–700 (2011).

193. R. I. M. Dunbar, S. Shultz, Evolution in the social brain. *Science* **317**, 1344–1347 (2007).

Acknowledgments: We are indebted to Duncan Haldane, Erin Brandt, Leeann Louis, and Heather More for their significant contributions to foundational work on this project, and to Robert J. Full and Steve Collins for insightful critiques at early stages.

Funding:

National Science Foundation award 1924303 (SAB, TL)

National Science Foundation award 2045014 (SAB)

Air Force Office of Scientific Research grant FA9550-22-1-0315 (SS)

Dunn Family Endowment (SS)

Army Research Office grant W911NF-23-1-0039 (KJ)

Meta Foundation (KJ)

NSERC Discovery Grant RGPIN-2020-04638 (JMD)

Author contributions:

Conceptualization: TL, JMD

Data curation: SAB, TL, KJ, SS, JMD

Visualization: SAB, TL

Writing – original draft: SAB, JMD

Writing – review & editing: TL, KJ, SS, JMD

Competing interests: Authors declare that they have no competing interests.

Data availability: All data are available in the main text or the supplementary materials.

Supplementary Materials

Supplementary Text

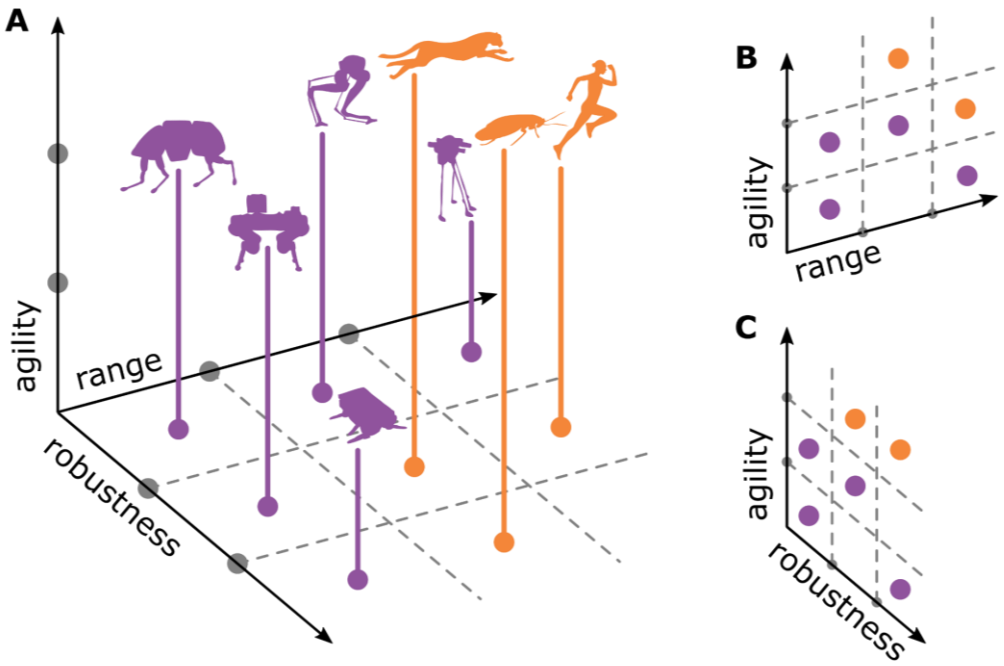

Fig. 1. System-level performance of animal and robot runners. (**A**) Representative performance of robots (purple) and animals (orange) in the three-dimensional space defined by *range*, *agility*, and *robustness* axes. (**B**) Projection of (A) onto agility-range plane. (**C**) Projection of (A) onto agility-robustness plane. Animal running performance currently Pareto-dominates that of robots at all scales.

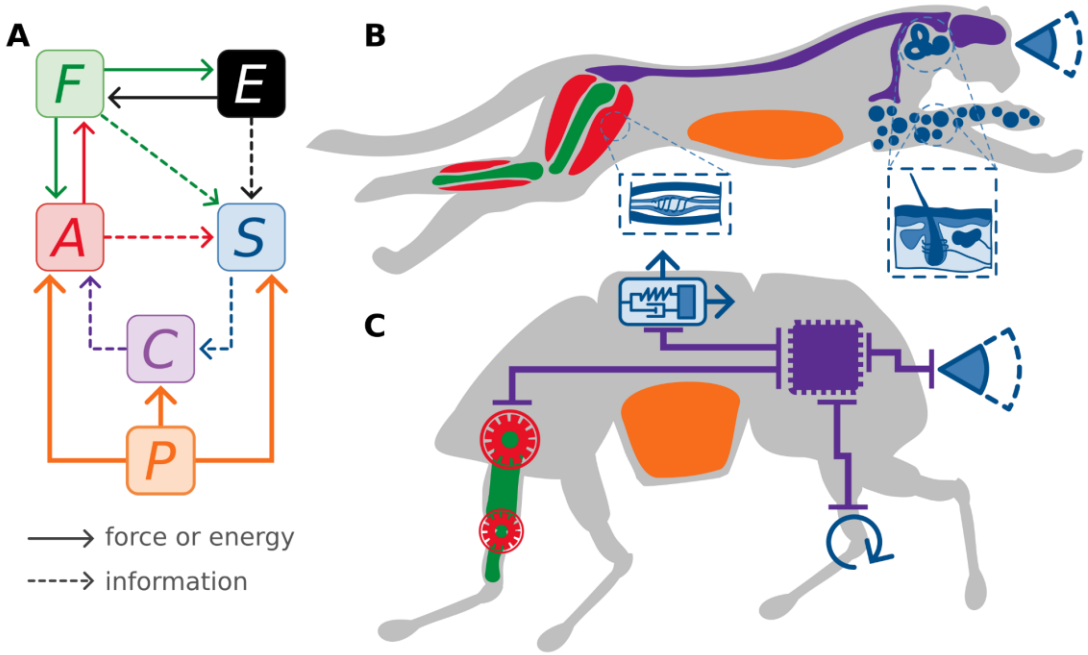

Fig. 2. Five subsystems critical for running. (**A**) Block diagram showing interconnections between the ***P****ower,* ***F****rame*, ***A****ctuation*, ***S****ensing*, ***C****ontrol* subsystems as they interact with the ***E****nvironment* (green, red, blue, purple, orange, and black, respectively). Solid arrows indicate transduction of force or energy, dashed arrows indicate transmission of information. (**B**) Illustration of the five subsystems overlaid on the fastest running animal (*Cheetah*): fat and metabolism; bone skeleton; muscles; visual, vestibular, and proprioceptive sensors; nervous system. (**C**) Illustration of the five subsystems overlaid on the fastest autonomous running robot (*WildCat*): gas engine or electric battery; metal or carbon fiber struts; hydraulic or (piezo)electric motors; vision, IMU, and joint sensors; computer network.

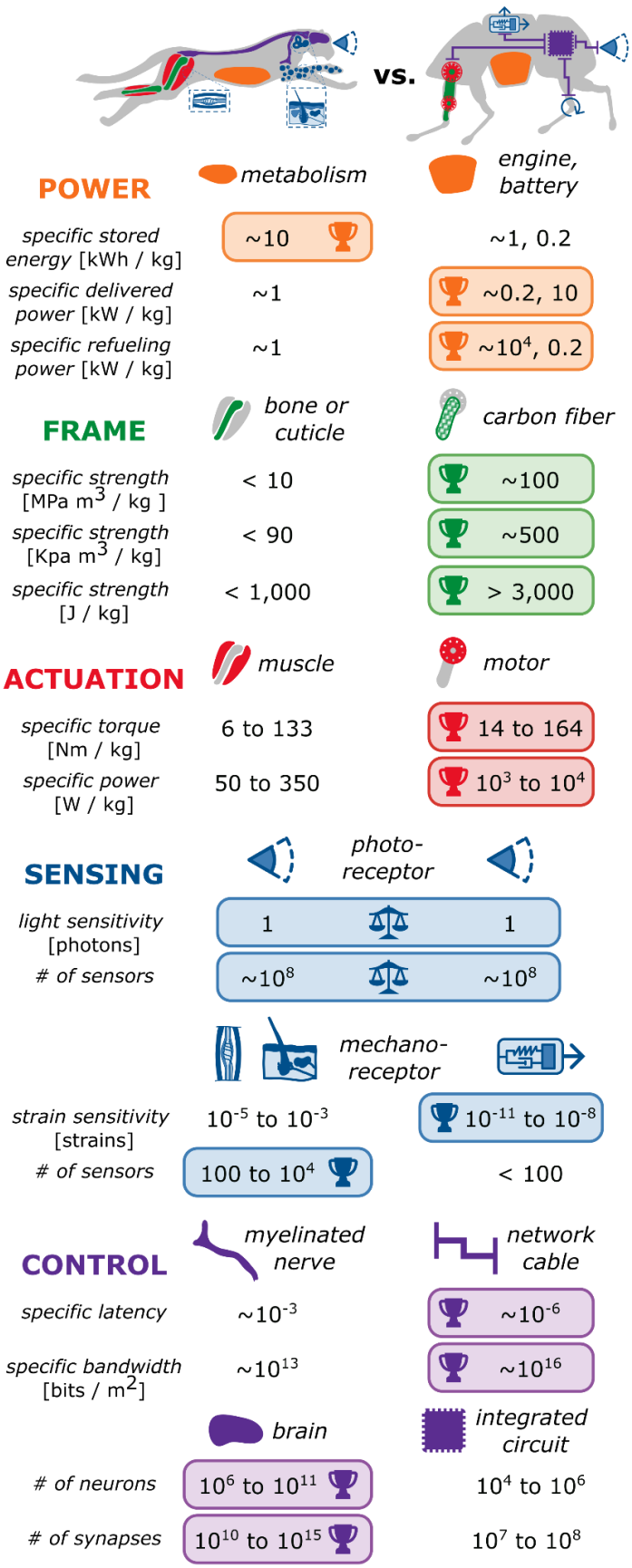

Fig. 3. Subsystem-level performance of animal and robot runners above 1kg. Performance in each subsystem is compared using multiple performance metrics and one or more engineering technologies. A trophy icon denotes when one technology outperforms another; a balanced scale icon denotes comparable performance. (See SM for comparisons at smaller scales.)

Science
AAAS

Supplementary Materials for

Why animals can outrun robots

Samuel A. Burden, Thomas Libby, Kaushik Jayaram, Simon Sponberg, J. Maxwell Donelan

Corresponding author: sburden@uw.edu

The PDF file includes:

Supplementary Results
Tables S1 to S41

Supplementary Results

This supplement summarizes the quantitative comparisons we made between animals and robots in the five subsystems critical for running: power, frame, sensing, actuation, and control.

The following table summarizes the results of our quantitative comparisons across subsystems between biological and engineered technologies. Each subsystem has an associated color (orange for power, green for frame, red for actuation, blue for sensing, purple for control) that is used in the table to highlight technologies that perform best with respect to each metric. This color is also used in the sections that follow to highlight the specific data tables that are used to populate the summary table. In some subsystems, all tables will be colored; in others, intermediate calculations and datasets are used to derive the quantities that populate the summary table, so those intermediaries are not colored.

			Biological	*Engineered*	
Subsystem	**Metric**	**Units**	**Metabolism**	**Gas engine**	**Electric battery**
POWER	*Mass-specific stored energy*	kWh / kg	6.7	2.7	0.2
	Mass-specific delivered power	kW / kg	1.2	0.2	10.9
	Mass-specific refueling power	kW / kg	0.8	28,500.0	0.2
	Metric	**Units**	**Bone, Cuticle**	**Carbon fiber**	**Aluminum, steel**
FRAME	*Density-specific stiffness*	MPa m^3 / kg	< 10	71.0	< 30
	Density-specific strength	KPa m^3 / kg	< 90	516.1	< 200
	Mass-specific energy	J / kg	< 1000	3753.7	< 1200
	Metric	**Units**	**Muscle**	**Electric motor**	**Bimorph piezo**
ACTUATION	*Mass-specific peak torque*	Nm / kg	6 to 133	14 to 164	11
	Mass-specific power	W / kg	50 to 350	1000 to 10,000	160
	Metric	**Units**	**Photoreceptor**	**Photoreceptor**	

SENSING	*Light sensitivity*	photons	1	1	
	# of sensors	#	1.00E+08	1.00E+08	
		Units	**Mechanoreceptor**	**Mechanoreceptor**	
	Strain sensitivity	strain	1E-5 to 1E-3	1E-11 to 1E-08	
	# of sensors	#	1E+2 to 1E+4	1E+01	
	Metric	**Units**	**Myelinated nerve**	**Network cable**	
	Period-specific latency	(none)	4.15E-03	4.58E-06	
Communication	*Area-and-period specific bandwidth*	bits / m^2	2.50E+13	9.72E+15	
CONTROL		**Units**	**Brain**	**Integrated circuit**	
Computation	*# of neurons*	#	1E+06 to 8.6E+10	1E+04 to 1E+06	
	# of synapses	#	1E+10 to 1E+15	1E+07 to 2.56E+08	

Table S1. Summary of quantitative comparisons. Values and ranges for metrics defined in main text reported for biological and engineered technologies.

Power subsystem performance

Body mass fraction

Our aim in this section is to quantify what fraction of the mass of fully-functional runners – such as a human or an autonomous legged robot – is composed of the power system. We treat the energy storage mass fraction separately and consider the mass fraction required for refueling and energy conversion together. We do so as the mass required for energy storage can change depending upon the range requirements, and indeed does so throughout the lifespan, or throughout an extended migration, in biological runners.

For the purpose of making our calculations understandable, we use the following masses to represent animals that are approximately the size of a cockroach, a cat, and a human.

	Body mass M [kg]
Cockroach	0.005
Cat	5
Human	100

Table S2. Representative body masses for cockroach, cat, and human.

Metabolism

What should we consider as the complete subsystem? One approach would be to look at the minimum mass of the storage (fat), energy conversion (mitochondria), and refueling (digestion) components. Although they are not runners, a complete power subsystem of this nature is present in unicellular organisms. Alternatively, we could look at the smallest legged insects or the smallest terrestrial mammals (shrews). Here are some interesting numbers for these possibilities: A single mitochondrion has a mass on the order of 4E-17 kg, a single cell has about 300 mitochondria on average, and the smallest unicellular organisms are on the order of 1E-15 kg (*107*). The smallest beetles and spiders are on the order of 1E-6 kg (*108*). The smallest terrestrial mammals (shrews) are on the order of 1E-3 kg (*87*).

Biological power systems can be made on extremely small scales. Here, rather than consider how small this subsystem can be made, we consider what fraction of the mass it comprises in different sized animals.

For mammals, mitochondria as a fraction of body mass scales with $0.06\,M^{-1/4}$ where the units of M are kg, which we will write as $[M]$ = kg (*107*).

	Mitochondria body mass fraction [(none)]
Cockroach	0.226
Cat	0.040
Human	0.019

Table S3. Body mass fraction of mitochondria in cockroach, cat, and human.

Franz *et al.* have the wet gastro-intestinal (GI) tract mass scaling as $0.075\,M^{0.94}$ for 41 species (mass range not reported) (*109*). The same reference has lizard GI tract mass scaling as $0.031\,M^{1.159}$ for 29 species with a range of body masses 0.008–1.123kg. Gordon and Illius studied African ruminants and found a greater fraction of the body mass dedicated to digestion, as might be expected due to the nature of what they eat and how they extract energy from it. They found $0.100259\,M^{1.1}$ for 21 species with an approximate mass range of 3.7--807 kg (*110*). Here we use Franz's mammal scaling relationship as the coefficient falls between the three possibilities, and $[M]$ = kg for all preceding formulas.

	GI tract body mass fraction [(none)]
Cockroach	0.103
Cat	0.068
Human	0.057

Table S4. Body mass fraction of gastrointestinal tract in cockroach, cat, and human.

To determine the fraction of body mass dedicated to energy conversion and refueling, we add the mitochondria mass to the gastro-intestinal tract mass.

	Conversion and refueling body mass fraction [(none)]
Cockroach	0.329
Cat	0.108
Human	0.076

Table S5. Body mass fraction of conversion and refueling components in cockroach, cat, and human.

The mass of body fat in eutherian terrestrial mammals versus total body mass scales with $0.075\,M^{1.19}$ ($[M]$ = kg) (*111*).

A sample of Madagascar hissing cockroaches, *Gromphadorhina portentosa*, has a body mass of 9.59 grams and a measured fat mass of 0.15 grams (*112*). This equates to about 2% of body mass as fat, which is consistent with the mammalian values.

	Body fat mass fraction [(none)]
Cockroach	0.016
Cat	0.102
Human	0.180

Table S6. Body mass fraction of fat in cockroach, cat, and human.

Gasoline

We use *BigDog* as a representative gas-powered runner, which has a mass of 109 kg (*113*).

The refueling hardware on the robot is quite light as it mainly consists of the pipe/hose that leads to the gas tank. We don't have good values for this mass, but we also didn't think it is important as the refueling rate is many orders of magnitude higher than the biological system so any plausible mass will not change the comparison. Here we neglect it.

From a presentation report, we know the component mass including engine, drive, pump, heat exchanger, and oil tank is 21.4 kg. In addition, we know the mass of a full tank of fuel is 5.68 kg, consisting of 4.73 kg of fuel and 0.955 kg of fuel tank.

	Body mass M [kg]	**Engine and fuel mass [kg]**	**Body mass fraction [(none)]**
BigDog (*113*)	109.000	27.109	2.49E-01

Table S7. Body mass fraction of engine and fuel for BigDog robot.

Batteries

Batteries differ from biological power and gasoline power in that the mass dedicated to refueling, conversion, and storage is integrated into one component, making it difficult to separate the individual component masses. The batteries typically used for robots have a fairly consistent amount of energy per unit mass. Consequently, what determines their contribution to total body mass is the capacity of the battery selected by the robot designers, and the mass of the body components that are not dedicated to power. Here we will use a representative sample of autonomous battery-powered robots to estimate the typical fraction of body mass that the battery-powered system comprises.

Similar to the refueling hardware in gas engines, the mass of the power electronics used to charge and discharge batteries is small relative to the battery mass, so we neglect it here.

	Body mass [kg]	**Battery mass [kg]**	**Body mass fraction [(none)]**
MIT Cheetah 2015 (*114*)	33.00	3.00E+00	9.09E-02
MIT Cheetah 2018 (115)	45.00	3.00E+00	6.67E-02
ETH StarlETH 2014 (116)	25.00	2.58E+00	1.03E-01

ETH ANYmal 2016 (117)	30.00	3.00E+00	1.00E-01
Average	3.33E+01	2.90E+00	9.02E-02

Table S8. Body mass fraction of batteries for quadrupedal robots.

The values are fairly consistent, so we will use the average in what follows.

As a final note, the *Cornell Ranger 2012* robot (*11*), which was designed to set range records, had a body mass of 9.9 kg and an estimated battery mass of 2.3 kg, equating to 23% of body mass dedicated to battery – more than double the other robots that were not designed to maximize range alone.

Specific stored energy

Metabolism

Stored fat has 39.5 MJ / kg (*118*). Fat is stored in fat cells (adipocytes) which are 87% fuel (lipids) and 13% other material (*48*). Mitochondria converts stored fat into ATP with an efficiency that can vary, with 70% being a good approximation (*46*).

	Mass-specific stored energy [kWh / kg]
Metabolism	6.682

Table S9. Mass-specific stored energy for metabolism.

Gasoline

The mass-specific chemical energy of gasoline is 13 kWh/kg (*54*). Combining this quantity with the fuel mass of *BigDog* yields a stored energy of 61.5 kWh.

To determine specific stored energy, we consider the energy delivered, rather than that of the raw fuel, because there are efficiency losses in the conversion of energy stored in the fuel's chemical bonds to the potential and kinetic energy of a robot's limbs. Dunn-Rankin *et al.* present a range of efficiencies for automotive engines (~25–30%) with efficiency going down with size (*47*). Since the engine in *BigDog* is on the small side, here we will use 25% efficiency. Note that this figure captures the conversion of stored chemical energy to the mechanical energy output of the engine as this is what we aim to quantify with our metric. The tank to wheel efficiency is lower, ~13% (*54*). See also Figure 18 in (*47*).

The mass-specific stored energy for *BigDog* is thus the fuel energy (in kWh) divided by the sum of the fuel and tank mass (in kg) multiplied by the efficiency of converting that gasoline chemical energy into engine mechanical energy.

	Mass-specific stored energy [kWh / kg]
BigDog	2.704

Table S10. Mass-specific stored energy for BigDog robot.

Batteries

Here we focus on lithium-polymer (LiPo) batteries as they are commonly used in running robots. The reported specific energies tend to range between 0.1–0.3 kWh/kg. Other practical battery technologies can have higher specific power (*119*).

	Mass-specific stored energy [kWh / kg]
MIT Cheetah 2015 (*114*)	1.55E-01
MIT Cheetah 2018 (115)	2.17E-01
ETH StarlETH 2014 (116)	1.72E-01
ETH ANYmal 2016 (117)	2.17E-01
Average	1.90E-01

Table S11. Mass-specific stored energy for quadrupedal robots.

Again there is modest variation in the values. We report the value for the *MIT Cheetah 2018* robot battery as it was designed more recently than the others and the associated publication reports a complete set of specifications for the battery performance.

Specific delivered power

Metabolism

Weibel and colleagues, as summarized by Suarez *et al.*, have found that the maximum rate of oxygen consumption by mammalian mitochondria is 5 ml/min per cubic centimeter of mitochondria (*120*), essentially independent of animal size. The energy consumed per ml of O_2 is 21 J (*121*). To obtain the delivered power, we need to account for the efficiency of transforming consumed energy into ATP. As we noted earlier, this efficiency is ~70% (*46*). If we assume that 1 ml of mitochondria weighs 1 gram, we can solve for specific delivered power.

	Mass-specific delivered power [kW / kg]
Metabolism	1.225

Table S12. Mass-specific delivered power for metabolism.

Gasoline

The delivered engine power in the *BigDog 2018* robot is quoted as 15 hp. The power delivered by the hydraulic actuators is reduced by conversion inefficiencies. But comparing the delivered engine power to the power delivered by ATP or electricity by batteries seems most reasonable.

	Mass-specific delivered power [kW / kg]
Gasoline	0.175

Table S13. Mass-specific delivered power for gasoline.

Batteries

The LiPo robot batteries described in the previous section have discharge rates (C-rates) of 40, 45 and 100. C-rate measures the rate at which a battery is discharged relative to its maximum capacity. Here we will report the specifications for the *MIT Cheetah 2018* robot battery as above, which has a C-rate of 50. A 50C rate means that the discharge current will discharge the entire battery in 1/50 hour. We don't correct for conversion inefficiencies as this is already included in the C-rate calculation.

	Mass-specific delivered power [kW / kg]
Battery	10.850

Table S14. Mass-specific delivered power for batteries.

Specific refueling power

Metabolism

Resting metabolic rate famously depends on body size according to Kleiber's law. For mammals, we will use $0.0182\,M^{0.737}$ ($[M]$ = g) (*122*). We are assuming that the resting metabolic rate is well approximated by the basal metabolic rate (basal rate is lower than resting rate). Across a wide range of vertebrates, Diamond and Hammond determined that animals can sustain a metabolic rate that is between 1.3-7.0 times their resting metabolic rate (*123*). This sustained rate is the maximum metabolic power they can sustain without losing weight. Here we approximate the ratio of the sustained to resting metabolic rate as 5. Finally, we normalize by the masses of the digestive system which is our approximation of the hardware that is responsible for fueling in biological runners.

	Mass-specific refueling power [kW / kg]
Cockroach	2.89E-04
Cat	7.11E-02
Human	7.74E-01

Table S15. Mass-specific refueling power for cat, cockroach, and human.

Gasoline

The rate of refilling a gas tank in a consumer car is a controlled standard, and the energy liberated from gasoline is also well known. Previously we assumed the mass of the refueling hardware was negligible – for the purpose of this calculation, we assume it is 1 kg. The resulting quantity is consistent with the figure in (*47*).

	Mass-specific refueling power [kW / kg]
Gasoline	28,500

Table S16. Mass-specific refueling power for gasoline.

Batteries

The LiPo robot batteries described in the *Specific Stored Energy* section have charge rates of between 1 and 5C. This measures the rate at which a battery is charged relative to its maximum capacity. Here we will report the specifications for the battery in the *MIT Cheetah 2018* robot (*115*) as we have a complete battery data set and the specifications are similar to the other comparison robots and hobbyist batteries. We don't know its exact charge rate, but let's assume it is 1. A 1C rate means that the charge current will charge the entire battery in 1 hour.

	Mass-specific refueling power [kW / kg]
Battery	0.217

Table S17. Mass-specific refueling power for battery.

Frame subsystem performance

A robot or animal's frame is the primary means of mechanical interaction with its environment, propelling the body forward while overcoming gravity. During these interactions, the frame is subject to substantial dynamic forces that often exceed the body weight depending on the locomotion modality (*124*). For example, peak forces during constant average speed human running are typically twice the body weight (*125*). But, during dynamic movements like jumping, they can exceed over 100 times for small animals (*126*). These interactions can result in the structural or functional failure of a frame. Our motivation is to define a set of possible metrics to capture the performance limits that frames might impose on the agile movement.

Material and shape

We consider frames as structures, combining material properties (for instance, strength, stiffness, density) and shape (for instance, length, section modulus, moment of area) to support loads and restrict or control motion. Viewed at the level of a component, such as a leg segment, shape and material are independent but interacting factors that together determine structural performance. This coupling must be taken into account when analyzing this subsystem.

To illustrate this challenge, we first consider a foundational function of a runner's limb: support the body's weight. As a first approximation to understand a limb's mechanical properties, consider a thin-walled tube (such as a bone or strut). When subject to axial forces, such a column can fail either by axial compression or buckling as determined by the following governing expressions. For a detailed discussion on this topic, we refer the readers to the comprehensive textbook by Ashby (*127*), specifically Appendix A5 on page 482.

During *axial compression*, the governing equation is

$$\sigma_{ax} = \frac{F}{A} < Y$$

where:

- σ_{ax} is the compressive stress;
- F is the axial force;
- A is the cross section area; and
- Y is the compressive strength (Yield or Ultimate).

During *buckling*, the governing equation is

$$\frac{F_{cric}}{A} = \frac{\pi\lambda^2 E}{2(L/R)^2}$$

where:

- F_{cric} is the critical force after which buckling occurs;
- A is the cross section area;
- λ is the half wavelength signifying the buckling mode;
- L is the column length; and
- R is the gyration radius.

The above expression for compressive stress can be rewritten as,

$$\sigma_{bk} = K\frac{E}{s^2} < Y$$

where:

- σ_{bk} is the compressive stress;
- K is a proportionality constant determined by the bending mode;
- E is the elastic (Young's) modulus *(a material factor)*;
- s is the slenderness ratio *(a shape factor)*; and
- Y is the compressive strength (Yield, Ultimate, or Modulus of Rupture as appropriate for elastic, plastic, or brittle materials).

These constraints highlight the strong interdependence of material and shape in determining the performance of a frame element.

Failure of a column will occur in purely axial compression if the stress (σ_{ax}) in the column reaches the yield stress (Y) of the material *(strength-dominated)*. On the other hand, if the critical buckling stress (σ_{bk}, determined by the modulus E) is less than the yield stress (Y), then the column will fail by buckling before yield stress is reached *(stiffness-dominated)*.

Our subsequent analyses will focus specifically on thin-walled tubes. We believe this simplification is reasonable because thin-walled tubes are remarkably common in the diversity of bones across vertebrates or tibia across insects (*128*). Choosing one specific shape enables us to focus on the *material* properties of biological and engineered frames without having to simultaneously consider the *shape*. Methods to incorporate the effect of shape are discussed in detail as 'shape indices' in Chapters 5 and 11 of (*127*).

We will focus on material indices that determine a limb's functional performance primarily dependent on stiffness (E) and strength (Y) as discussed above. Furthermore, we assume that we want the lightest possible limbs for reducing actuation and power subsystem constraints and therefore we normalize these material properties by their density (D). Thus, we will consider *density-specific stiffness* ($M1 = E/D$) and *density-specific strength* ($M2 = Y/D$), which both contribute to the above failure modes. We compute these for common biological (bone and cuticle) and robotic (aluminum and carbon fiber) materials. We also include Stainless Steel, a popular engineering material for various non-robotic applications, for contrast. Below is the range of material properties derived from (*55*, *59*, *127*, *129*).

	Stiffness *E* [GPa]	**Strength *Y* [MPa]**	**Density *D* [10^3 kg/m^3]**
Cuticle	0.001-120	10-1200	1-1.3
Cortical bone	7-30	100-230	1.8-2.1
Tendon	1-2	50-150	1.1-1.2
Natural rubber	0.0015-0.0025	22-32	0.92-0.93
Kevlar	76	1240	1.38

CFRP (carbon fiber reinforced plastic)	69-150	550-1050	1.5-1.6
Aluminum	68-82	58-550	2.5-2.9
Stainless Steel	180-210	480-2240	7.6-8.1

**approximate due to small data points and/or large variance.*

Table S18. Stiffness, strength, and density ranges for biological and engineered materials.

Note that Kevlar and natural rubber are examples of specialized materials as described in Metric 3 (below) and not used for Metrics 1 & 2.

We choose typical numbers within the above range to evaluate our metrics.

	Stiffness *E* [GPa]	**Strength *Y* [MPa]**	**Density *D* [10^3 kg / m^3]**
Cuticle	9	100	1.15
Cortical bone	19	165	1.95
Tendon	1.5	100	1.15
Natural rubber	0.002	26	0.92
Kevlar	76	1240	1.38
CFRP	110	800	1.55
Aluminum	75	302	2.7
Stainless Steel	195	1350	7.85

**approximate due to small data points and/or large variance*

Table S19. Representative stiffness, strength, and density values for biological and engineered materials.

Specific stiffness

It is straightforward to compute this metric from the preceding data tables. Carbon fiber outperforms all other materials by a wide margin.

	Density-specific stiffness *M1* = *E* / *D* [MPa m^3 / kg]
Cuticle	7.8
Cortical bone	9.7
Tendon	1.3
CFRP	**71.0**
Aluminum	27.8
Stainless Steel	24.8

Table S20. Density-specific stiffness for biological and engineered materials.

Specific strength

Similar to the previous metric, it is straightforward to compute this metric from the data tables. Carbon fiber outperforms all other materials by a wide margin.

	Density-specific strength *M2* = *Y* / *D* [KPa m^3 / kg]
Cuticle	87.0
Cortical bone	84.6
Tendon	87.0
CFRP	**516.1**
Aluminum	111.9
Stainless Steel	172.0

Table S21. Density-specific strength for biological and engineered materials.

Specific energy

The preceding metrics focused on the frame's ability to support the body's weight. We now combine these metrics to evaluate the performance of frames as they propel the body overground. In this capacity, an important function of the frame is to store and return energy for increasing the range of locomotion – the frame should function as a spring. We assess a spring's ability to store and release mechanical energy using the material's capacity to store energy defined as the area under the stress-strain curve of the material and normalized by density. This material metric is defined by the following equation, which also relates it to the previous two metrics.

$$M3 = \frac{Y^2}{ED} = \frac{M2^2}{M1}$$

	Mass-specific energy $M3 = Y^2 / E * D = M2^2 / M1$ [J / kg]
Cuticle	966.2
Cortical bone	734.8
Tendon	**5797.1**
Rubber	*367391.3*
Kevlar	*14660.6*
CFRP	3753.7
Aluminum	450.4
Stainless Steel	1190.6

Table S22. Mass-specific energy for biological and engineered materials.

Carbon fiber again outperforms bone, cuticle, aluminum, and steel in this metric. However, tendon outperforms carbon fiber. This is not surprising given that tendon's remarkable role in energy storage and release during energy-intensive locomotion is well-documented (*130*, *131*).

However, there are other engineering materials with more exceptional performance if we consider this metric alone. For example, Kevlar has more than twice the mass-specific energy of tendon, and natural rubber is nearly an order of magnitude better than Kevlar by this metric. However, tendon, Kevlar, and rubber have low specific stiffness and are therefore much less effective for load-bearing than the other materials considered. These springy materials are best employed within the frame to add specific functionality like passive energy storage and return.

Actuation subsystem performance

A dazzling array of technologies have been deployed in the quest for an actuator that could equal or exceed muscle in the pursuit of robotic running. It is a daunting prospect to collect comparative metrics for all of them. Luckily, to substantiate our hypothesis we need not do so. Here we compare the only natural technology for actuating running (muscle) to the most ubiquitous engineered actuator, electric motors, and find that except at small scales, electric motors can perform similarly or substantially better than muscle. At smaller scales, we compare muscle to the most commonly used solution for autonomous microrobots, the piezo bimorph. We find piezos slightly lacking in comparison to muscles at the same scale, but within a similar order of magnitude.

Overview of technologies

Some general principles constrain the types of actuators available for running. By definition runners have legs, and although simple machines might use prismatic (*132*) or flexible structures (*133*), most animals and robots use jointed structures with multiple segments. Thus we consider an actuator for running to be a device that generates rotary motion around a joint. Linear actuators like muscle accomplish this with a moment arm, which affords some torque-speed adjustment at design time.

Muscles are hierarchical molecular machines in a matrix of elastic material. They produce a tension force by inducing a conformational change (via a chemical reaction with ATP) in a myosin protein, which then ratchets along another protein. Despite the universality of muscle as Nature's actuator, maximum stress and power values range widely, even within the same organism. As in engineered actuators, muscles exhibit specialization for tasks (for instance, some may be slow but strong, others the opposite). In all muscles, force falls nearly logarithmically with shortening speed, producing a maximum power near 1/3rd the maximum speed. They have a density near water and have intrinsic stiffness much lower than the metals that comprise EM motors.

Electric motors vary in their construction and mechanism of operation but generally harness the Lorentz force that arises when a current-carrying wire is placed in a magnetic field. They typically spin much faster than joints need to during legged locomotion, so EM motors benefit from speed-reducing transmissions. Unlike muscle, EM motor torque need not fall with increasing speed, if voltage is high enough.

Piezo bimorphs are cantilever actuators consisting of two active piezo crystal layers sandwiching a passive flexible layer. When an electric field is applied, the cantilever bends; mechanical output is taken at the tip of the cantilever (*134*). Piezos typically require relatively high voltages, so power electronics can be a challenge at small scales.

Since running necessitates repeated collisions with the ground, the effective inertia at the foot is extremely important. The bandwidth of high-speed impacts is typically much faster than that of the actuator, so impact forces are not directly controllable and energy loss is inevitable (*135*). Thus actuators must be fairly backdrivable and must isolate as much inertia as possible from the

end effector. This precludes many transmission approaches like worm gears, lead screws, and harmonic drives unless some compliance is added between the joint and the transmission.

Specific peak torque

In the context of running, actuators most frequently create motion by applying torque at joints. Since stronger actuators tend to weigh more, we first compare *mass-specific peak torque*.

Muscle

Values for muscle can be found from direct experiments, or more commonly by making assumptions about the maximum stress available in combination with measurements of area and moment arm. Maximum muscle force can be calculated by the product of stress and area; in the biological literature area is often estimated by physiological cross-sectional area, defined as the ratio of muscle volume and fiber length. Therefore, *mass-specific torque* can be estimated by the product of the maximum stress and moment arm over the product of fiber length and density.

This calculation assumes parallel fibers; a correction for pennation can be added by dividing the specific torque by the cosine of the pennation angle (*136*). Muscles with large moment arms and short fiber length will maximize specific torque. The ratio (moment_arm/fiber_length) varies from 0.1 to 0.3 in the cockroach hind limb (*137*), from 0.3 to 1.0 in the human lower limb (*138*), and generally from 0.1 to 1.0 in the greyhound (*136*), though more extreme values are found for postural muscles especially. Combined with a representative value of maximum stress of 20 N / cm^2, this rough calculation suggests a possible range of ~20 to 200 Nm / kg in running animals. Values found in the literature for invertebrates, dogs, and humans lie within that interval.

	Mass-specific peak torque [Nm / kg]
Cockroach hind limb extensors (*137*, *139*)	10-60
*Hunting spider flexo*r (*140*)	30

Table S23. Mass-specific peak torque for insect muscle.

An extensive set of morphological data in the greyhound provides insight into a range of hindlimb muscles in one of the fastest known runners (*136*). Direct force measurements were not available, and a constant specific force (stress) of 30 N / cm^2 was used to estimate muscle forces. The larger muscles have remarkably low torque density, suggestive of specializations for high shortening velocity and high power production in fast running. Some smaller muscles with much larger fiber length to moment arm ratios like gracilis and gastrocnemius reach values of 33–47 Nm / kg. Data from the three largest muscles are below.

	Mass-specific peak torque [Nm / kg]
Greyhound biceps femoris	6
Greyhound sartorius	10

Greyhound rectus femoris	7.5

Table S24. Mass-specific peak torque for dog muscle.

In humans, values arise from measurements of (typically) volitional maximum isometric torque collected on an isokinetic dynamometer, combined with morphometrics collected from MRI or ultrasonography, often combining muscle groups across a joint because humans can't selectively activate single muscles reliably (*141*, *142*).

	Mass-specific peak torque [Nm / kg]
Human elbow flexors (141)	133
Human elbow extensors (141)	100
Human ankle extensors (142)	120

Table S25. Mass-specific peak torque for human muscle.

Electric motor

Direct drive machines have a distinct disadvantage in torque density. Flux saturation limited direct drive motors can reach values of ~25 Nm / kg with large gap radius designs (*23*). Adding low-ratio gearboxes (typically single-stage planetary) can improve torque density further.

Higher ratio gearboxes can increase torque density but have diminishing returns due to the added weight of the drive. One popular approach, especially in robot arms, is to use Harmonic drives, also known as strainwave gears, which use a novel flexible spline ring gear to produce very high ratios in a compact single-stage drive. Ratios beyond 100:1 are common. Multi-stage planetary drives and cycloids are alternatives. To meet the backdrivability requirement, all high-ratio drives must use series elastic elements. Walking robots with stiff, high-ratio drives typically exhibit stiff gaits and high cost of transport (ASIMO for instance, which uses harmonic drives with no series compliance).

Converting an electric motor's torque to linear motion (for instance, via ball-screw mechanism) and back to rotary joint torque via moment arm is another popular approach that results in very high torque density.

	System type or configuration	**Total Motor + Transmission Mass [kg]**	**Torque [Nm]**	**Mass-specific peak torque [Nm / kg]**
T-Motor U8 (23)	Direct drive	0.25	3.5	14
MIT Cheetah 2017 (*143*)	Gearbox (5.8:1), no SEA	3.65	313.2	86
DLR FSJ Variable Stiffness Joint (144)	Harmonic drive (100:1), SEA	1.41	67	48

Harmonic drive + Robodrive LM (Not likely capable of running, included for comparison) (145)	Harmonic drive (100:1), no SEA	1.8	182	101
Univ. Texas UT-SEA, with a moment arm of half the stroke (6cm) (66)	Ball-screw with series coil spring	1.17	84	72
MIT TF8 Ankle; omitting ankle structure (*146*)	Ball-screw with series leaf spring	1.064	175	164

Table S26. Mass-specific peak torque for electric motor.

Piezo bimorph

At very small scales, electric motors see dramatically reduced power and torque density. Some of the most well known high-performance microrobots use piezo bimorphs for actuating wings or legs. The robot HAMR-jr (*147*) (smaller successor to HAMR (*148*)) uses 24 mg bimorphs to achieve torque density below muscles found in cockroaches but above those found in greyhounds. The bimorph motion is amplified with a linkage that is integrated into the limb; therefore we omit the linkage mass.

	System type or configuration	**Motor mass [kg]**	**Torque [Nm]**	**Mass-specific peak torque [Nm / kg]**
Piezo bimorph with flexures (*147*)	Flexure linkage with mechanical advantage	2.40E-05	2.70E-04	11

Table S27. Mass-specific peak torque for piezo bimorph.

Specific power

Since running is dynamic, torques must be generated over a wide range of speeds. A common way to compare this ability is through mechanical power (the product of speed and torque). Again, more powerful motors are heavier, so we compare *mass-specific power*.

Muscle

Since power amplification mechanisms abound (for instance, latch-mediated springs (*68*)), the gold standard for measurements is the workloop (*149*) – an in vitro technique that cycles isolated muscle or its subcomponents while applying electrical stimulation, analogous to a motor dynamometer. The technique allows the full performance space to be explored, including muscle activation and phase that are not part of the typically observed motor pattern. Here we consider power averaged over a whole cycle, since instantaneous power may reflect elastic energy storage and return. Specific power values found via this technique still vary over ~2 orders of magnitude, especially between vertebrates and invertebrates (*150*). The highest known value comes from

quail flight muscle. Values for limbs are generally lower, but this number gives an "existence proof" of extreme power adaptation to compare against.

When these invasive techniques are not available (for instance, in humans), estimates exist for muscle groups across a joint. Joint power can be measured with an isokinetic dynamometer or other instrument, or during behaviors that generate mechanical work (for instance, acceleration or climbing)

Note that muscle is single-acting and antagonistic in most animals; over one cycle of motion, a kilogram of muscle can only contribute power while shortening (for instance, during extension only), whereas a kilogram of electric motor produces power in both directions (i.e., flexion and extension). In many cases, muscles even actively absorb power while their antagonist works, especially when cycling quickly. Although muscles may instantaneously produce higher power levels (for instance, over 1000W/kg for quail flight muscle (*151*)), instantaneous values make for a misleading comparison. Therefore, we use cycle-averaged power in the following comparison.

	Measurement method	**Mass-specific power [W / kg]**
Quail flight muscle (*151*)	Workloop	350
Lizard (149)	Workloop	150
Mouse (152)	Workloop	107
Frog hindlimb extensor (*153*)	Workloop	94
Locust hindlimb extensor (*151*)	Workloop	75
Cockroach hindlimb extensor (139)	Workloop	50
Turkey hindlimb (154)	Acceleration; whole hindlimb mass used	150
Human knee extensors (155)	Cycle dynamometer; test duration 5-10 minutes	117

Table S28. Mass-specific power for muscle.

Electric motor

Electric motors produce torque proportional to the supplied current, up to a maximum typically determined by magnetic saturation (or more practically, due to heat build up). Unlike muscles, motors do not experience intrinsic reduction in force with increased velocity, unless supply voltage is limited. Like muscle, motors can be specialized, trading torque, maximum speed, and other parameters, so performance values vary. Because high currents can heat a motor quickly, the maximum torque and power can be very sensitive to the time horizon. Still, many papers cite “maximum” numbers, and we will use those here. At the highest speeds, mechanical limits arise due to centripetal forces.

Compared to muscle, electric motors can generate extremely high power densities, typically at high rotary speed. Even over longer time horizons, motors can sustain high power density. Values near 1 kW / kg can be found for continuous power in commercial off-the-shelf motors. When integrated into structures with high ratios, power density can be substantially degraded (especially when power supplies are limited), but values still typically meet or exceed that of muscle.

	System type or configuration	**Motor mass [kg]**	**Power [W]**	**Mass-specific power [W / kg]**
Typical direct-drive 3-phase motors (135)	Direct drive	(*see ref*)	(*see ref*)	1000-10,000
Maxon EC frameless DT50	Direct drive	0.225	150	667
DLR FSJ Variable Stiffness Joint (144)	Harmonic drive (100:1), SEA	1.41	600	426
Univ. Texas UT-SEA, with a moment arm of half the stroke (6cm) (66)	Ball-screw with series coil spring	1.17	110	94
MIT TF8 Ankle; omitting ankle structure (146)	Ball-screw with series leaf spring	1.064	350	329

Table S29. Mass-specific power for electric motor.

Piezo bimorph

Piezo bimorphs can generate high power at high frequencies, but may be more limited in limb structures with lower resonant frequency. HAMR's actuators resonate at 1600 Hz, generating over 300 W/kg, but when integrated into a robot resonate at 75 Hz and generate only 38 W/kg. HAMR-Jr's legs resonate at higher frequencies, enabling about 4X more power density of 160 W/kg, substantially more than its biological inspiration.

	System type or configuration	**Motor mass [kg]**	**Power [W]**	**Mass-specific power [W / kg]**
Piezo bimorph with flexures (*156*)	Flexure linkage with mechanical advantage	2.40E-05	3.84E-03	160

Table S30. Mass-specific power for piezo bimorph.

Sensing subsystem performance

Our motivation is to capture the performance limits that sensors might impose on the generation of controlled, agile movement. Biological sensing is classically partitioned into exteroception and proprioception. But the former strictly is the sensing of external cues, whereas the latter is typically defined as the sensation of self-movement, pose, and internal mechanical state. As a result, these are not a true dichotomy. Internal sensing can be chemically mediated and the detection of external cues through force transmitted through the body such as vibration and load sensing belie this partition. An exoskeletal strain receptor or even a muscle stretch receptor could therefore detect deformations produced by self-motion or respond to externally applied forces, especially during unsteady movement. Nonetheless, it is a useful heuristic for discussing the use case of sensors in behavior. Interestingly such a dichotomy does not seem to exist in the engineering literature, likely because specific sensors are often designed to capture only specific single modalities. In these cases, roboticists often design control of specific task variables to utilize a specific few sensory modalities leading to dichotomies like force versus positional control that do not align with organisms' typically multimodal strategies.

The most common metrics for sensors in engineered systems are sensitivity and resolution. The former is a ratio of the change in the sensor to the sensor output. The resolution is the smallest amount of change in the input that can be resolved as a change in the output. Similar definitions have been used in the biological literature with the output of a sensory neuron often quantified by the firing rate of action potentials or the membrane potential of the neuron. A challenge with comparing sensitivity and resolution across systems is that their values are context-dependent: they can depend both on the design of the sensors themselves, the power supplied, and the situation in which they are deployed.

Threshold sensitivity

We define *threshold sensitivity* as the minimum amount of input needed to register a detectable change in the sensor's output. The units depend on the type of sensors (for instance, photons, nm, concentrations).

Photoreceptors

Vision thresholds are defined by the number of photons needed to produce a response. Both invertebrates and vertebrates can achieve single photon thresholds with quantized bumps in their photoreceptor's membrane potential (*71*). The best engineered semiconductor photodiodes can also achieve this resolution (*72*).

	Photoreceptor threshold sensitivity [#]
Vertebrates & Invertebrates	1 photon
Single Photon Avalanche Diodes (SPAD)	1 photon

Table S31. Biological and engineered photoreceptor threshold sensitivity.

Mechanosensors

For mechanosensation there are a larger variety of ways to measure displacement or deformation, but both biological and engineered systems often rely on strain ($\varepsilon = \Delta L/L$). Campaniform sensilla are typically between 10^1 and 10^2 μm and have a detection threshold of 10 nm (*73*). Mammalian hair cells are used in both audition and vestibular sensation, with some modifications. Auditory hair cells can resolve displacements down to 0.3 nm and at 10^1 to 10^2 μm is size, this gives a threshold sensitivity of ~10^{-5} strain (*157*). However, Brownian motion at these scales is often ~1–3 nm (*158*) so the actual limit may be thermodynamic at ~10^{-4} strain. Most engineered strain sensors can achieve better threshold strain sensitivities from 10^{-8} to 10^{-11} but are often longer in absolute size by design in order to achieve this (*159*). So, the absolute threshold in both cases may again be down to biophysical limits of thermal noise.

	Mechanosensor threshold strain sensitivity [(strain)]
Cockroach campaniform sensilla	1E-03
Guinea Pig hair cells	1E-05
Engineered strain sensors	1E-11 to 1E-08

Table S32. Biological and engineered mechanosensor threshold sensitivity.

Number of sensors

Our second metric is the number of sensors. This is a common sensor metric (sometimes reported as a density, for instance, pixels / cm^2) and draws an important distinction between biological and engineered runners.

Photoreceptors

For vision, the number of sensors is just the number of photoreceptors in the eye. In invertebrate compound eyes, each facet is called an ommatidium (plural: ommatidia) and each has usually between 6–10 photoreceptors (*160*).

	Number of photoreceptors [#]	**Explanation**
Biological:		
Cockroach *Periplaneta americana (76)*	1.4E4	2000 ommatidia, 7 photoreceptors per ommatidium
Fly *Drosophila melanogaster (161)*	5.6E3	700 ommatidia, 8 photoreceptors per ommatidium
Moth *Paysandisia archon (162)*	1.8E5	20,000 ommatidia, 9 photoreceptors per ommatidium
Feather-wing beetle *Ptiliidae (163)*	~4E2	~50 ommatidia, 8 photoreceptors per ommatidium

Human *Homo sapiens (157)*	1E8	
Engineered:		
100 MP camera (engineering)	1E8	found in high-end smartphones

Table S33. Biological and engineered number of photoreceptors.

Mechanosensors

Quantifying the total number of mechanosensors for animals is very species specific and in the case of mechanoreceptors it is unclear if the appropriate comparison point is all mechanosensors or only those thought to be used in proprioception. Such distinction is likely to be important for investigations of specific systems, but our broad point is captured by a very general comparison.

	Number of mechanosensors [#]
Insect campaniform sensilla (79)	1000 to 10,000
Insect chrodontonal organs (79)	Many with 100s of sensors per organ
Insect other mechanosensitive hairs and sensilla (79)	100 to 10,000
Human tactile receptors (77)	20,000
Human muscle spindles (164)	5,000
Angular encoders (engineering)	< 100; typically equals # of degrees-of-freedom

Table S34. Biological and engineered number of mechanosensors.

Perceptual threshold

It is important to draw a distinction between the threshold sensitivity of the sensor and the behavioral or perceptual threshold, which is the smallest unit of input that an organism can perceive consciously (i.e. discriminate when asked) or respond to behaviorally. For vision, perceptual thresholds can still occur at the single photon level (*165*), but for mechanosensation, they are typically much higher than the threshold sensitivity (*166*). However, these perceptual limits are a consequence of the integration of sensing, control, and behavior rather than of fundamental limits on the sensors themselves.

	Perceptual threshold about a limb joint [deg]
Human elbow flexion (167)	1
Locust scratching (168)	< 10

Table S35. Perceptual threshold about a limb joint in human and locust.

Control subsystem performance

Since control consists of transmission and transformation of signals, we compare the communication channels and computational elements available to animals and robots.

Communication

Our goal is to quantify the bandwidth and latency of communication channels found in nervous systems and computer networks of runners. Before quantitatively comparing these metrics, we motivate their definition using fundamental performance constraints in control systems.

Data-rate Theorems

Latency and bandwidth constrain control system performance via *data-rate Theorems (85)* by placing lower bounds on the steady-state error that can be achieved by any controller.

Consider the discrete-time linear time-invariant system,

$$x^+ = A\,x + B\,u.$$

Since stable modes do not need to be stabilized by feedback, we assume without loss of generality that a change-of-coordinates has been applied to extract only the unstable modes for consideration, so all eigenvalues of A have magnitudes larger than 1.

Define the intrinsic entropy rate H

$$H = log_2|\ det\ A\ |.$$

Note that $H > 0$ since all eigenvalues of A have magnitude larger than 1 and the determinant of a matrix equals the product of its eigenvalues.

Theorem 1 and Proposition 1 in (*85*) tell us that:

- if the bandwidth R, measured in units of bits per sample, is smaller than the intrinsic entropy rate, so $R < H$, then the system cannot be stabilized;
- if $R > H > 0$ and the communication channel has latency (i.e. delay) $L > 0$, measured in units of samples, then the norm of the steady-state error is lower-bounded by a function that increases without bound as R and L increase.

These theoretical results comport with the intuition that a controller can perform better when more information (measured by R) is available more quickly (measured by L). Importantly, these performance constraints apply regardless of how the controller is implemented, so we compare bandwidth and latency of communication channels implemented in nervous systems and computer networks.

Application of data-rate Theorems

Consider the dynamics of an inverted pendulum,

$$m\,l^2\ddot{q} = m\,g\,l\ \ sin\,(q) + u,$$

where:

- m is the pendulum mass;

- l is the pendulum length;
- g is the acceleration due to gravity;
- q is the pendulum angle, $\dot{q}$ its velocity, $\ddot{q}$ its acceleration; and
- u is the control torque applied to the pendulum.

Since runners must be capable of maintaining an upright posture, stabilization of an inverted pendulum defined by the runner's mass and leg length is a simple representative control problem solved by a nervous system or computer network in a runner.

By time-discretizing the pendulum dynamics with sampling interval d and linearizing about the vertical equilibrium point, the intrinsic entropy rate can be shown to be

$$H = log_2(1 + d\sqrt{g/l}).$$

Note that this expression decreases as the natural frequency $\sqrt{g/l}$ of the pendulum increases. This finding comports with intuition, as larger runners have more time to correct for errors before they hit the ground, so less bandwidth is required to attain the same steady-state error (*169*). We normalize latency and bandwidth by the natural period $\sqrt{l/g}$ to obtain dimensionless quantities for comparison across scales.

	Leg length [m]	**Natural period [sec]**
Cockroach	0.02	0.284
Cat	0.25	1.003
Human	1	2.006

Table S36. Leg length and natural period of cockroach, cat, and human.

Specific bandwidth

The maximum bandwidth of a single axon is 1 kilobit per second; this bound has been posited theoretically (*170*) and measured empirically (*171*). Although the length of axons that approach this upper bound is generally much shorter than a cat's or human's leg length, this upper bound suffices for comparison with computer networks.

EtherCAT (IEC 61158) (*172*) is a standardized communication protocol for control systems that runs on CAT 5 Ethernet cables. This standard can update 100 servo axes with 16 bit precision every 100 microseconds for cable lengths up to 100 meters.

InfiniBand (*173*) is a proprietary communication protocol and medium for computer clusters that uses copper wires with lengths ranging from 0.5 to 1 meter and transmits data at up to 100 gigabits per second.

Many axons can be bundled into a single nerve, yielding a communication channel whose bandwidth theoretically scales linearly with the number of axons. However, the cross-sectional area of the channel also scales linearly with the number of axons, so we normalize bandwidth by cross-sectional area.

Axon diameters range from 0.2 to 20 micrometers in mammals (*174*, *175*), and there are theoretical reasons to believe smaller sizes are not practical (*176*), leading to a range of cross-sectional areas.

Ethernet wires range from 22 to 28 AWG, corresponding to diameters of roughly 0.5 mm, and the outer cable diameter is roughly 5mm.

Infiniband has 0.25 mm wires and roughly 10mm cable diameters.

To obtain a single representative diameter for subsequent calculations, we average these extremes. Since many orders of magnitude will separate the performance of a computer network from that of an axon, this choice does not influence the outcome of the comparison.

	Diameter [micrometer]		
	lower bound	*upper bound*	*representative*
Axon	0.2	20	10.1
EtherCAT	500	5000	2750
InfiniBand	250	10000	5125

Table S37. Diameter of axon, EtherCAT cable, and InfiniBand cable.

	Area-and-period-specific bandwidth [bit / m^2]
Axon	2.50E+13
EtherCAT	5.40E+12
InfiniBand	9.72E+15

Table S38. Area-and-period-specific bandwidth of axon, EtherCAT cable, and InfiniBand cable.

As a sanity-check for our rough calculations, we note that (*86*) estimates a bandwidth of approximately 10 megabits per second for the human retinal nerve, which has a 5 mm diameter (*177*), corresponding to an area-specific bandwidth of 5.09E+11.

This figure is lower than our estimate, but that outcome is unsurprising since we gave axons the advantage at every stage of the preceding calculation: we used the maximum theoretical bandwidth and didn't account for the adipose tissue (myelin) that insulates nerves, which can take up a substantial fraction of a nerve's area as summarized in Table B.1 of (*178*).

We find that a nerve (axon bundle) may theoretically outperform EtherCAT whereas having the same cross-sectional area, but there are faster communication protocols like InfiniBand that outperform the nervous system by two or more orders of magnitude.

Specific latency

Axonal conduction velocity is theoretically proportional to axon diameter; experimentally, conduction velocities top out at 120 m / sec for the myelinated nerves of terrestrial mammals (*179*, *180*) and 4 m / sec for the unmyelinated nerves of insects (*181*). Since latency is equal to distance divided by conduction velocity, signals transmitted the length of a runner's leg are delayed by more than a millisecond.

EtherCAT can update 100 servo axes every 100 microseconds for cable lengths up to 100 meters.

InfiniBand latency is 1.3 microseconds for cables up to 1 or 2 meters.

	Period-specific latency of *communication* [(none)]	**Notes**
Biological:		
Cockroach	1.76E-02	
Cat	2.08E-03	
Human	4.15E-03	
Engineered:		
EtherCAT	3.52E-04	*scale-invariant; cockroach natural period used to get worst-case value*
InfiniBand	4.58E-06	

Table S39. Period-specific latency of communication for axon, EtherCAT cable, and InfiniBand cable at cockroach, cat, and human length scales.

We find that EtherCAT may outperform axons by an order of magnitude in time required to transmit a signal the length of a runner's leg, and InfiniBand is hundred times faster still. It is impractical for animals to approach the latencies of computer network protocols, since doing so would require scaling up axon diameters by multiple orders of magnitude (*87*, *180*), which would not fit inside legs.

Computation

Our goal is to quantify the complexity of computations that can be performed in runners and the time required for the computation.

Intuitively, a controller's computation consists of transforming sensor signals to actuator signals. Mathematically, this transformation is a function. It is not clear what specific function or class of functions are necessary for high-performance running – all we have is the proof-of-concepts in animals, whose transformations are implemented in (biological) neural networks.

Robots have access to artificial and spiking neural networks in neuromorphic integrated circuits (*182*) as well as the fundamentally different von Neumann architecture (*183*). It is conceivable that digital computers based on von Neumann architectures could meet or exceed the

performance of animals' neural networks in their implementation of effective controllers, but in the absence of robots that are better at running than animals, we focus on the most direct comparison between natural and artificial spiking neural networks.

As a brief aside, it is worth noting that the von Neumann architecture is inefficient at "simulating" a spiking neural network – a supercomputer simulation of a leaky integrate-and-fire network on the scale of the human cerebellum required 82,944 von Neumann CPUs and ran six hundred times slower than realtime (*184*).

We are thus motivated to compare natural and artificial neural networks: on the one hand because they are the only option for general-purpose computation in the nervous system; and on the other because they are capable of solving complex optimization problems (*88*) and they are universal approximators (*185*) – any function can be approximated to any desired degree of accuracy by a network with a sufficiently large number of "neurons" (termed *units*) and "synapses" (the weighted connections between units).

We will not consider neural network architecture here for two reasons. First, feedforward neural networks with only one "hidden" layer have the "universal approximation" property, so there is no theoretical advantage in terms of the complexity of transformations that can be represented by considering deep networks (*186*). Second, there appear to be no practical constraints on the architecture that can be implemented in neuromorphic circuits, so if a particular network were discovered that solved a control problem particularly well, current design and fabrication technologies ought to be able to reproduce the circuit in silicon, so long as a sufficient number of units and connections were available in the integrated circuit.

Instead, we will focus on the number of units and connections that can be implemented in a runner's neural network, since these counts place limits on the space of transformations available to the runner. But we first repeat our analysis of latency to confirm a similar separation in performance holds between engineered and biological networks.

Specific latency

In a feedforward neural network, a "computation" is performed when a vector of inputs is transformed to a vector of outputs. This process does not occur instantly and is instead proportional to the latency or characteristic time constant of the network's units (*88*). This latency is on the order of milliseconds for natural neurons (*88*) and can be shorter than microseconds for artificial neurons (*89*).

	Period-specific latency of *computation* [(none)]
Biological:	
Cockroach scale	3.52E-03
Cat scale	9.97E-04
Human scale	4.98E-04

Engineered:	
Cockroach scale	3.52E-06
Cat scale	9.97E-07
Human scale	4.98E-07

Table S40. Period-specific latency of computation for axon, EtherCAT cable, and InfiniBand cable.

We find, perhaps unsurprisingly, that artificial units in specialized integrated circuits can be activated several orders of magnitude faster than biological neurons. Decades of intensive research and development into the design and fabrication of integrated circuits by the semiconductor industry has yielded engineered units that dramatically outperform their biological counterparts in this regard.

Number of neurons and synapses in a spiking neural network

Neuromorphic integrated circuits are undergoing something of a renaissance in recent years, motivated in part by the impressive performance of large-scale neural network architectures on machine learning challenges in perception, language, and control.

Industry research labs have created chips with the largest numbers: IBM's TrueNorth (*187*), which has an area of 430 mm^2, has 1e6 neurons and 2.56e8 synapses. Intel's Loihi (*188*), which has an area of 60 mm^2, has 1.3e5 "leaky integrate-and-fire" (LIF) neurons and 2e6 1-bit synapses.

The numbers have been more modest in academic research labs, with Tianjic (*89*) having an area of 14.4 mm^2 containing 4e4 neurons and 1e7 synapses. But Tianjic was notably used to control an autonomous robot (electric bicycle), whereas applications of the industrial chips have focused on more general-purpose machine learning tasks (*189*, *190*).

In stark contrast, animal nervous systems have staggering numbers of neurons and synapses: cockroach nervous systems have 1e6 neurons and 1e10 synapses on a characteristic length scale of 0.5 mm (*191*); cat brains have 7.6e8 neurons and 1e13 synapses, and the largest linear dimension of the brain is 50 mm; human brains have 8.6e10 neurons and 1e15 synapses, and the largest linear dimension of the brain is 150 mm.

	Neurons [#]	**Synapses [#]**	**Length scale [mm]**	**Neurons [words]**	**Synapses [words]**
Biological:					
Cockroach	1.00E+06	1.00E+10	0.5	1 million	10 billion
Cat	7.60E+08	1.00E+13	50	760 million	10 trillion
Human	8.60E+10	1.00E+15	150	86 billion	1,000 trillion
Engineered:					

Tianjic	4.00E+04	1.00E+07	4	40 thousand	10 million
Loihi	1.30E+05	1.26E+08	8	130 thousand	126 million
TrueNorth	1.00E+06	2.56E+08	21	1 million	256 million
Supercomputer	6.80E+10	5.40E+12	100,000	68 billion	10 trillion

Table S41. Number of neural units and synaptic connections in biological and engineered spiking neural networks.

We find support for the colloquial understanding of animal brains being remarkable computing machines relative to integrated circuits, specifically in terms of the complexity of transformations that can theoretically be implemented. But in conclusion, we recall the obvious fact that animal brains are used for a staggering variety of tasks beyond sensorimotor control, so it is unclear how much brain is needed to achieve high performance in any particular task like running. There are many competing theories for whether and why bigger brains are better (*91*). One observation is that primate brain size correlates with social network size (*192*), motivating the "social brain hypothesis" (*193*) that bigger brains evolved primarily in service of interactions with others, rather than to increase proficiency in tasks like locomotion that much smaller brains perform extremely well.